Micellar-Colloidal Iron Oxyhydroxide-Integrated Hybrid-Composites Photocatalysts for Orthogonal Rhodium/Cobalt-Mediated NAD$^+$/NADH Cycling and Mediator-Free Boronic Acid Hydroxylation

Shaifali Mishra [a], Rajesh K. Yadav [a], Chandani Singh [b], Rehana Shahin, Kanchan Sharma, Vinay K. Mishra, Surendra K. Jaiswal, Sandeep Chaudhary [c], Tanmoy Tantra [c], Jin Ook Baeg [b]**

*[a]*Department of Chemistry and Environmental Science, Madan Mohan Malaviya University of Technology, Gorakhpur-273010, U.P., India. *E-mail: rajeshkr_yadav2003@yahoo.co.in*
*[b]*Korea Research Institute of Chemical Technology, 141 Gajeong-ro, Yuseong-gu, Daejeon, South Korea. *Email: jobaeg@krict.re.kr*

[c]Department of Medicinal Chemistry, National Institute of Pharmaceutical Education and Research, Raebareli (NIPER-R), Lucknow (UP)- 226002

Contents

1. General Remarks

Benzene-1,3,5-tricarbaldehyde (Btc), cetyltrimethylammonium bromide (CTAB), sodium dodecyl benzene sulfonate (SDBS), acetic acid, 30% aqueous ammonia, pH indicator paper, ethanol, $FeSO_4 \cdot 7H_2O$, melamine, phenylboronic acid, triethanolamine (TEOA), sodium mono and dibasic salts, β-NAD^+ cofactor, acetonitrile, petroleum ether, ethyl acetate, benzoquinone, 2-naphthylboronic acid, 4-chlorophenylboronic acid, 4-hydroxyphenylboronic acid, furan-3-boronic acid, 4-formylphenylboronic acid, 4-toylphenylboronic acid, 4-methoxyphenylboronic acid, cobalt(II) chloride hexahydrate ($CoCl_2 \cdot 6H_2O$), dimethylglyoxime ($dmgH_2$), acetone, dichloromethane (DCM), pyridine, sodium bicarbonate ($NaHCO_3$), sodium sulfate (Na_2SO_4), diethyl ether, methanol, alcohol dehydrogenase (ADH), acetaldehyde, and (pentamethylcyclopentadienyl)rhodium(III) dichloride dimer were purchased from Sigma-Aldrich and TCI Chemicals (India) and used as received without further purification. Deionized water was used in all reactions. Phosphate-buffered saline (PBS, pH 7.0) was prepared from mono and dibasic sodium and potassium salts dissolved in deionized water.

2. Methods and Instrumentation

UV-visible absorption and diffuse reflectance spectra (DRS) were recorded on a Shimadzu UV-1900i spectrophotometer. Fourier transform infrared (FTIR) spectra were collected on a Shimadzu IR-8000 spectrometer using KBr pellets. Electrochemical measurements were carried out with a CHI608E-220V electrochemical workstation. Thermal stability was evaluated using a TA Instruments SDT Q600 V20.9 (N_2, 900 °C; heating rate: 10 °C min^{-1}; flow rate: 40 mL min^{-1}). Powder X-ray diffraction (PXRD) patterns were obtained on a Rigaku SmartLab High-Resolution Diffractometer (Cu Kα radiation, $\lambda = 1.5406$ Å, 45 kV, 200 mA) over a 2θ range of 5-70°. X-ray photoelectron spectroscopy (XPS) spectra were recorded on an AXIS SUPRA (KRATOS) using a monochromatic Al-Kα X-ray source at 15KeV. Raman spectra were recorded using a Nanophoton RAMANforce spectrometer. Morphological features were examined by field-emission scanning electron microscopy (FE-SEM, Carl Zeiss ΣIGMA HD, 10 keV). Elemental composition was determined by energy-dispersive X-ray spectroscopy (EDS, Bruker Quantax 200 with Si drift detector). High-resolution transmission electron microscopy (HR-TEM) images were acquired using a UC-EF-TEM operated at 200 kV. An atomic force microscope (AFM) (Bruker) was used to measure the surface morphology and height of the roughness. ^{1}H NMR spectra were recorded on a Bruker AVANCE II + 300 MHz spectrometer using tetramethylsilane (TMS, $\delta = 0$) as the internal reference. Specific surface area and porosity were determined by N_2 adsorption-desorption isotherms using the Brunauer-Emmett-Teller (BET) method using the Quantachrome Autosorb iQ3.

3. Synthesis of Btc/M composite and Btc/M-FeOOH hybrid-composite in a micellar system

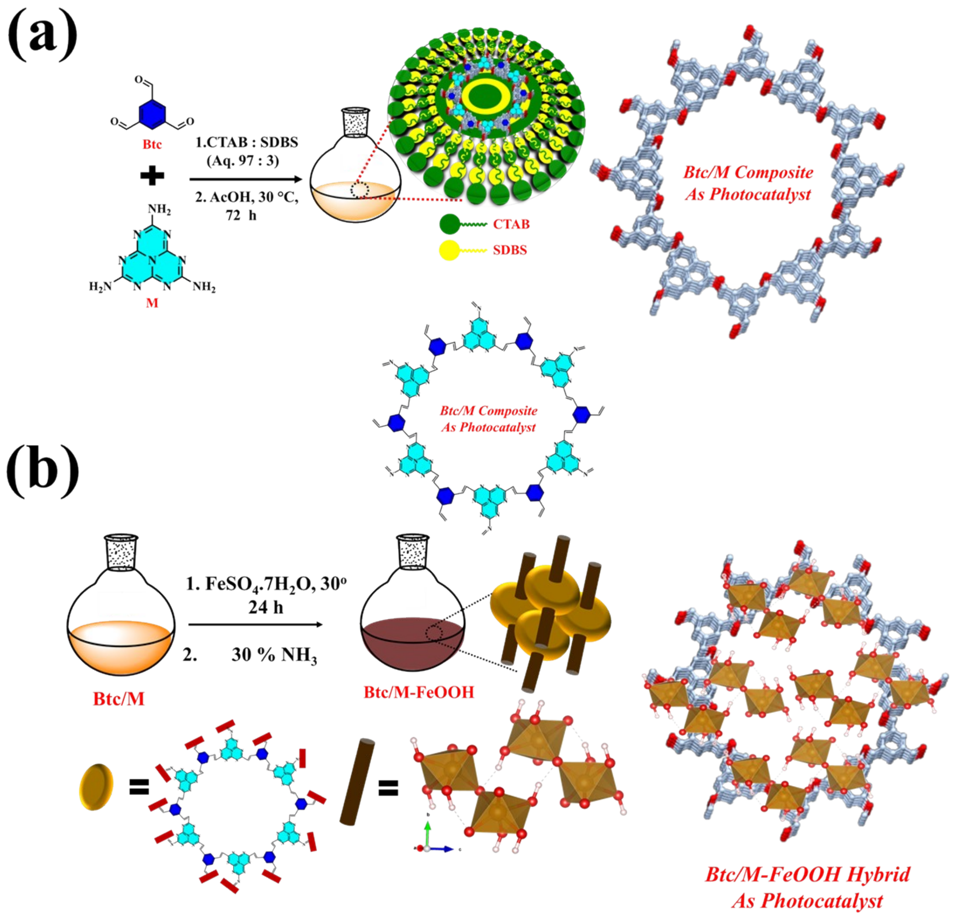

Figure S1. Synthesis of (a) Btc/M composite and (b) Btc/M-FeOOH hybrid composite via colloidal nanoparticle solution and subsequent flocculation, leading to crystalline frameworks. The structural diagram is a schematic representation of an idealized extended 2D periodic framework used to illustrate connectivity and pore architecture, and does not represent the minimal stoichiometric repeating unit.

4. Synthesis of Iron oxyhydroxide in a micellar system without Btc/M COFs

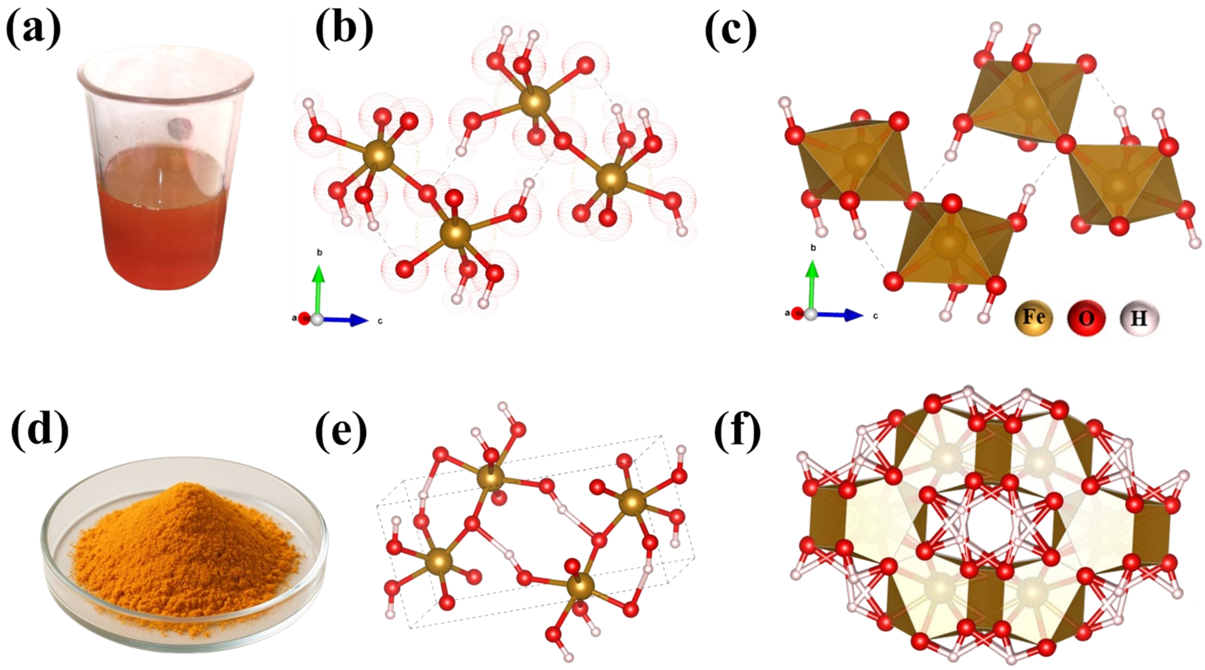

Figure S2. (a) Photograph of the colloidal goethite (α-FeOOH) solution and schematic representation of the (b) FeOOH coordination structure, (c) polyhedral network, (d) powdered FeOOH, (e) crystallographic unit cell of FeOOH, and (f) crystal framework of FeOOH displaying the tunnel-like arrangement of FeO_6 octahedra.

5. Synthesis of Co-Complex (Co-C)

To a solution of cobalt (II) chloride hexahydrate ($CoCl_2 \cdot 6H_2O$, 21 mmol) in 100 mL of acetone, a warmed solution of dimethylglyoxime ($dmgH_2$, 43.1 mmol) in 150 mL of acetone was added under continuous bubbling of air. The reaction mixture was stirred for 20 minutes and then allowed to stand at room temperature for 2 hours. Green crystals of [Co(dmgH)(dmgH_2) Cl_2] were obtained, which were filtered, washed, and dried to give a yield of 70.5%[1].

Subsequently, [Co(dmgH)(dmgH_2) Cl_2] (2.8 mmol) was dissolved in 10 mL of dichloromethane (DCM), followed by the addition of pyridine (2.8 mmol). To this solution, 10 mL of 0.1 N aqueous sodium bicarbonate ($NaHCO_3$) was added, and the mixture was stirred at room temperature for 1 hour. The reaction mixture was further diluted with 20 mL of DCM and washed with water (2 × 20 mL). The combined organic layers were dried over anhydrous sodium sulphate (Na_2SO_4), filtered, and evaporated to yield brown crystals of [Co$(dmgH)_2$Cl Py] with an isolated yield of 88.4%[1].

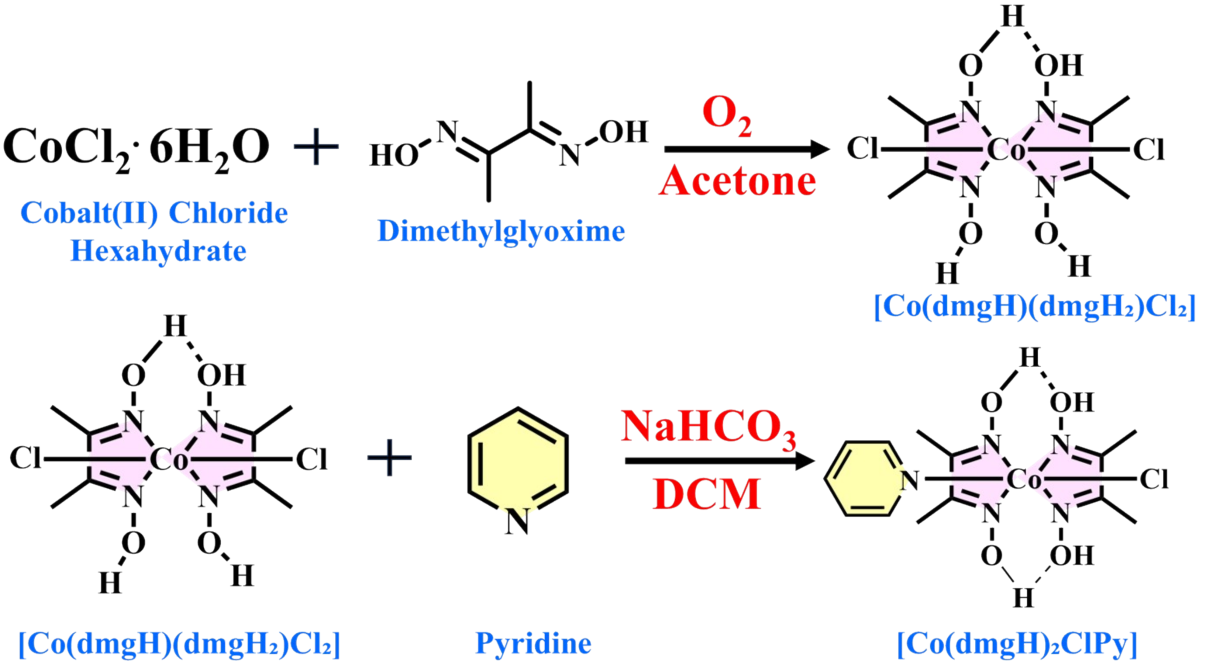

Figure S3. Synthesis of [Co(dmgH)(dmgH_2)Cl_2] and [Co$(dmgH)_2$ClPy].

6. Synthesis of Rh-Complex (Rh-C)

The synthesis of the Rh-C complex was carried out following previously reported protocols. Briefly, 25 mg of (pentamethylcyclopentadienyl)rhodium (III) dichloride dimer was dissolved in 5 mL of anhydrous methanol under an inert atmosphere and protected from light. To this solution, 13 mg of 2,2’-bipyridine (2 equivalents) was added, and the mixture was stirred in the dark. Upon completion of the reaction, diethyl ether was added to induce precipitation. A yellow-coloured solid was formed, which was collected and dried under ambient conditions[2,3].

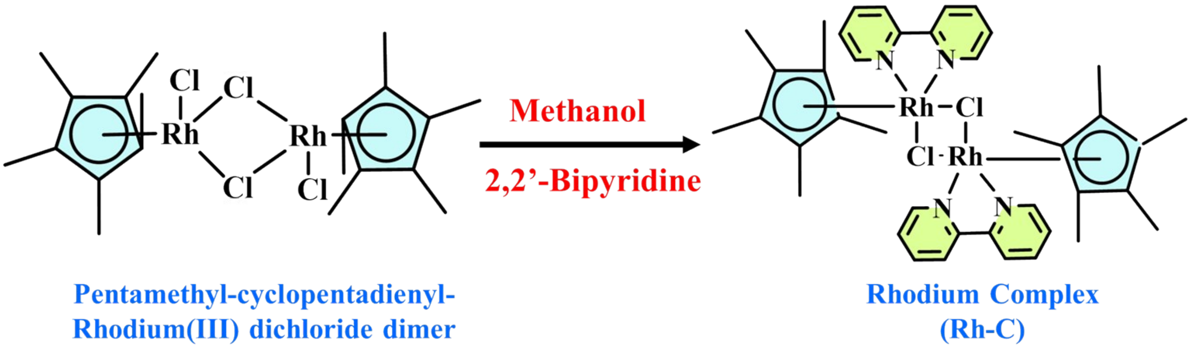

Figure S4. Synthesis of Rh-C.

7. UV-vis. Diffuse Reflectance Spectroscopy (UV-DRS)

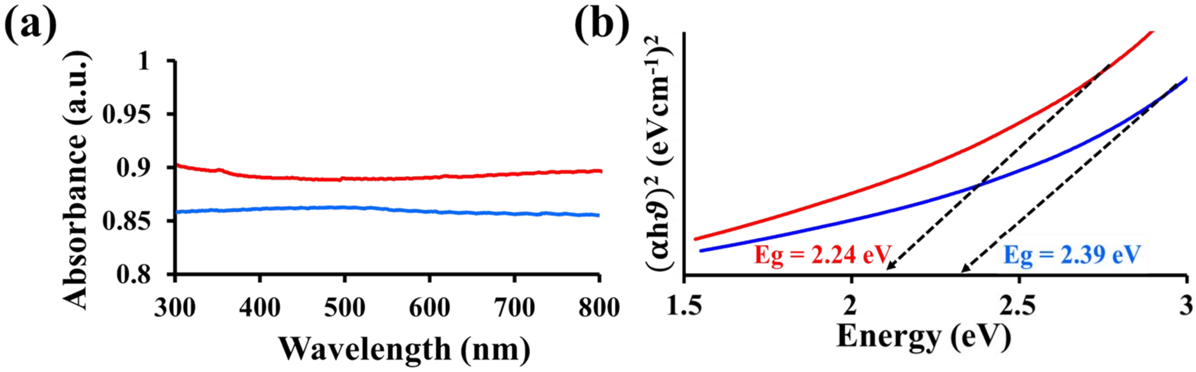

Figure S5. (a) UV-DRS spectra of Btc/M (blue) and Btc/M-FeOOH (red), and (b) Tauc plot of Btc/M (blue) and Btc/M-FeOOH (red).

8. Raman spectra of Btc/M

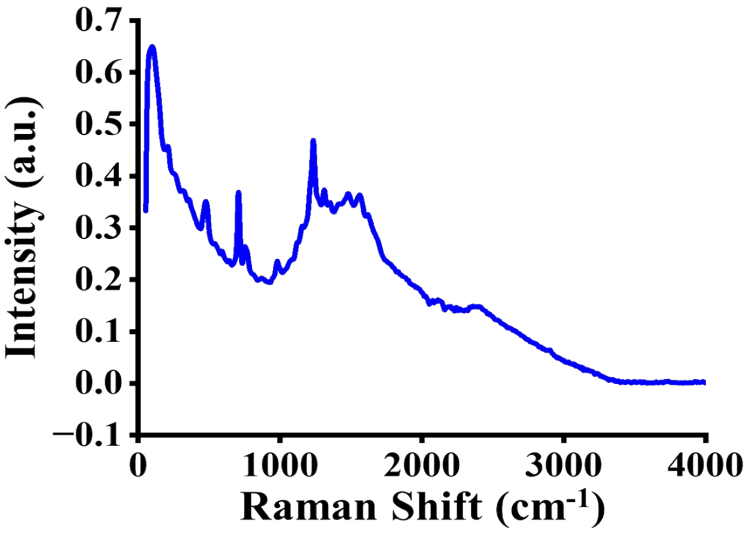

Figure S6. Raman spectra of Btc/M.

9. Cyclic Voltammetry of Btc/M and Btc/M-FeOOH

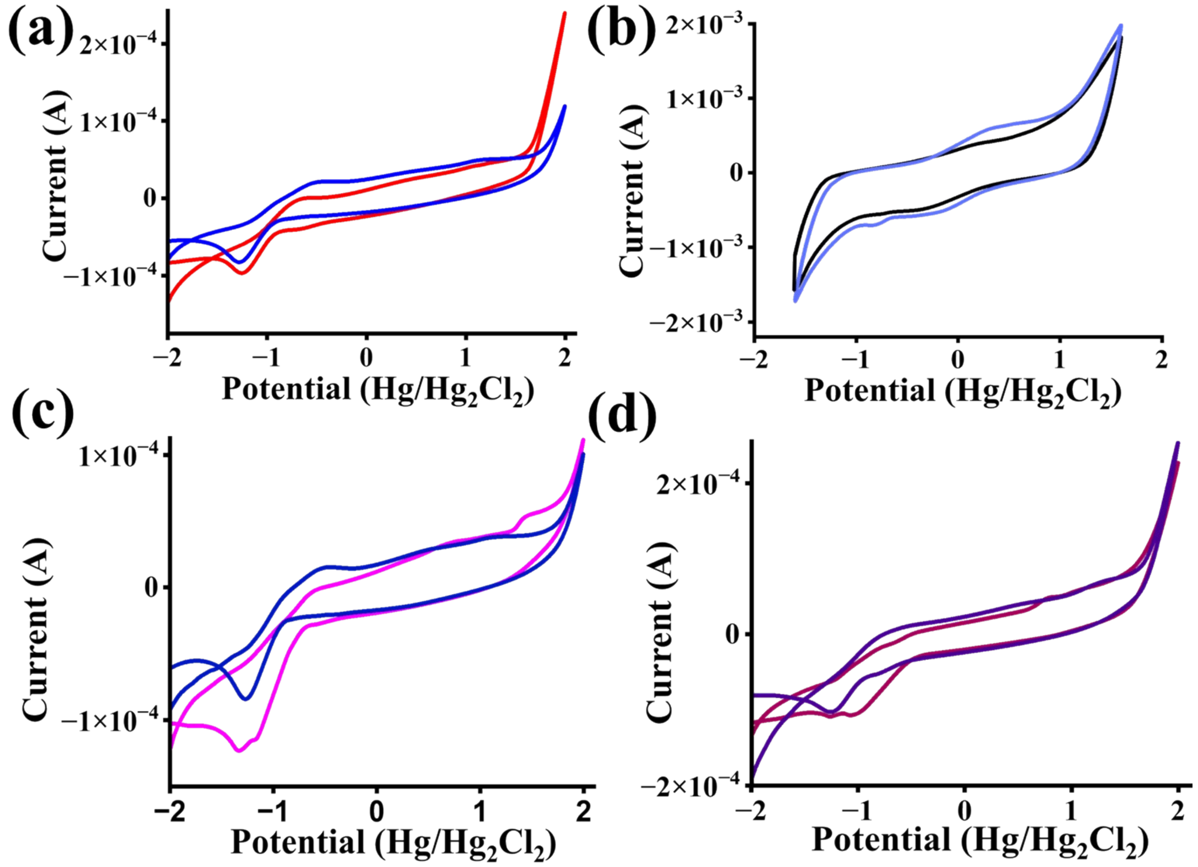

Figure S7. Cyclic voltammetry of (a) Btc/M (blue) and Btc/M-FeOOH (red), (b) Rh-C (black) and NAD$^+$ cofactor (blue), (c) Btc/M + Rh-C (blue) and Btc/M + Rh-C + NAD$^+$ cofactor, and (d) Btc/M-FeOOH + Rh-C (purple) and Btc/M-FeOOH + Rh-C + NAD$^+$ cofactor (dark pink).

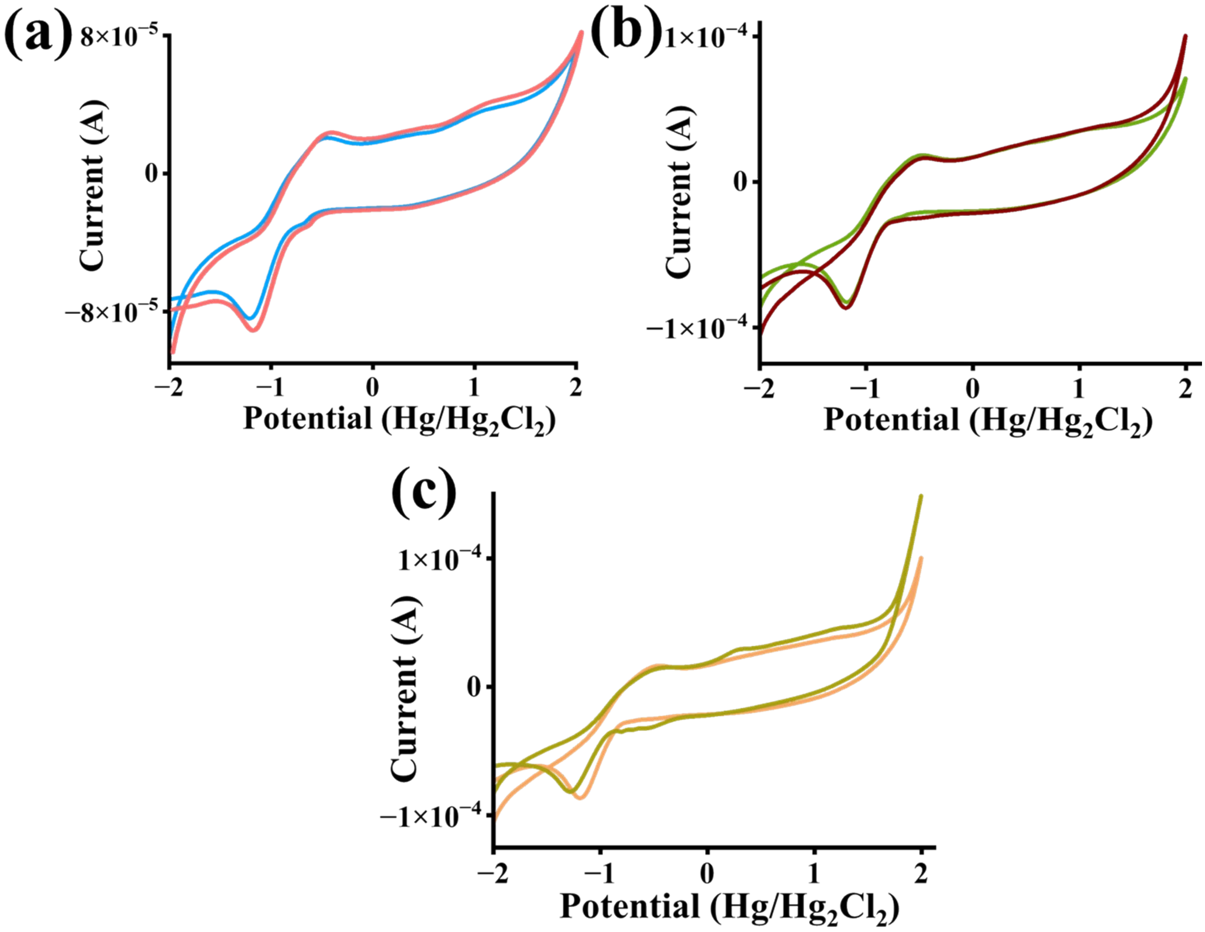

Figure S8. Cyclic voltammetry of (a) Co-C (blue) and Co-C + NAD$^+$ cofactor (red), (b) Btc/M + Co-C (green) and Btc/M + Co-C + NAD$^+$ cofactor (brown), and (c) Btc/M-FeOOH + Co-C (orange) and Btc/M-FeOOH + Co-C + NAD$^+$ cofactor (light green).

10. Electrochemical Impedance Spectroscopy (EIS), Tafel Plot, Mott-Schottky, and Chronopotentiometry (CP)

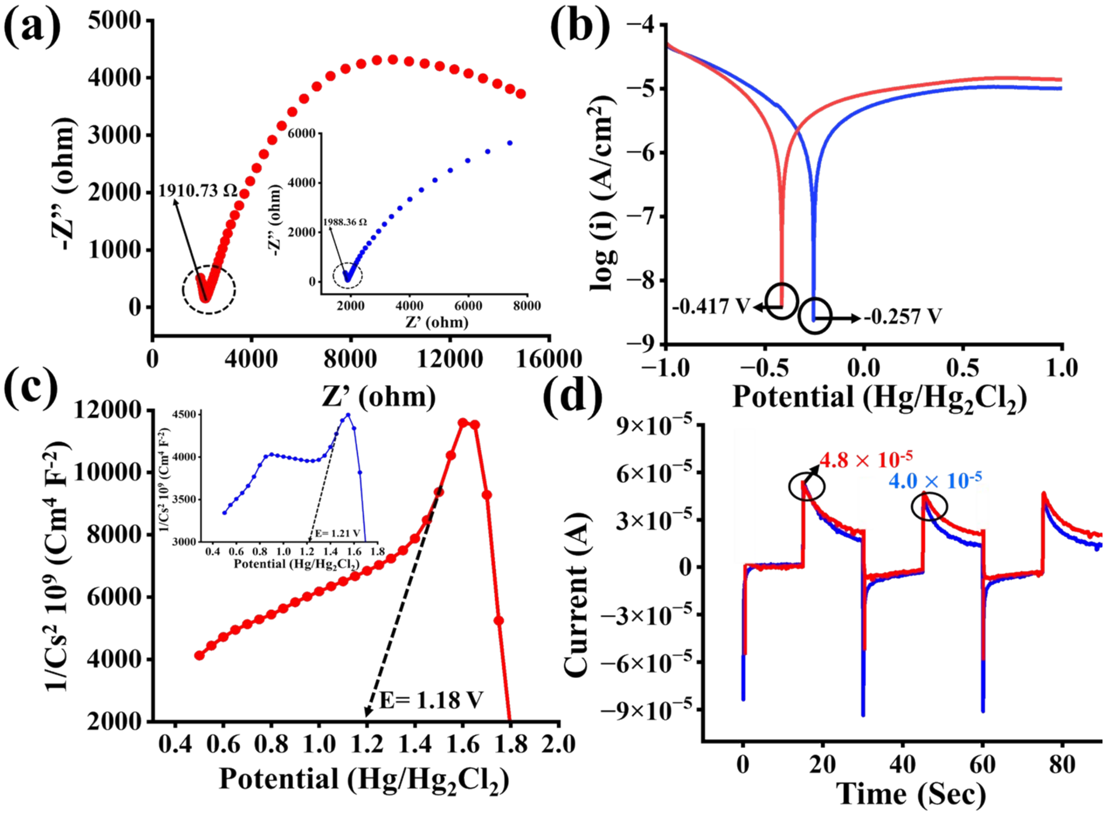

Figure S9. (a) EIS of Btc/M (blue) and Btc/M-FeOOH (red), (b) Tafel plot of Btc/M (blue) and Btc/M-FeOOH (red), (c) Mott-Schottky of Btc/M (blue) and Btc/M-FeOOH (red), and CP of Btc/M (blue) and Btc/M-FeOOH (red).

11. Surface Area and Porosity Analysis via Brunauer-Emmett-Teller (BET) and Nitrogen Sorption

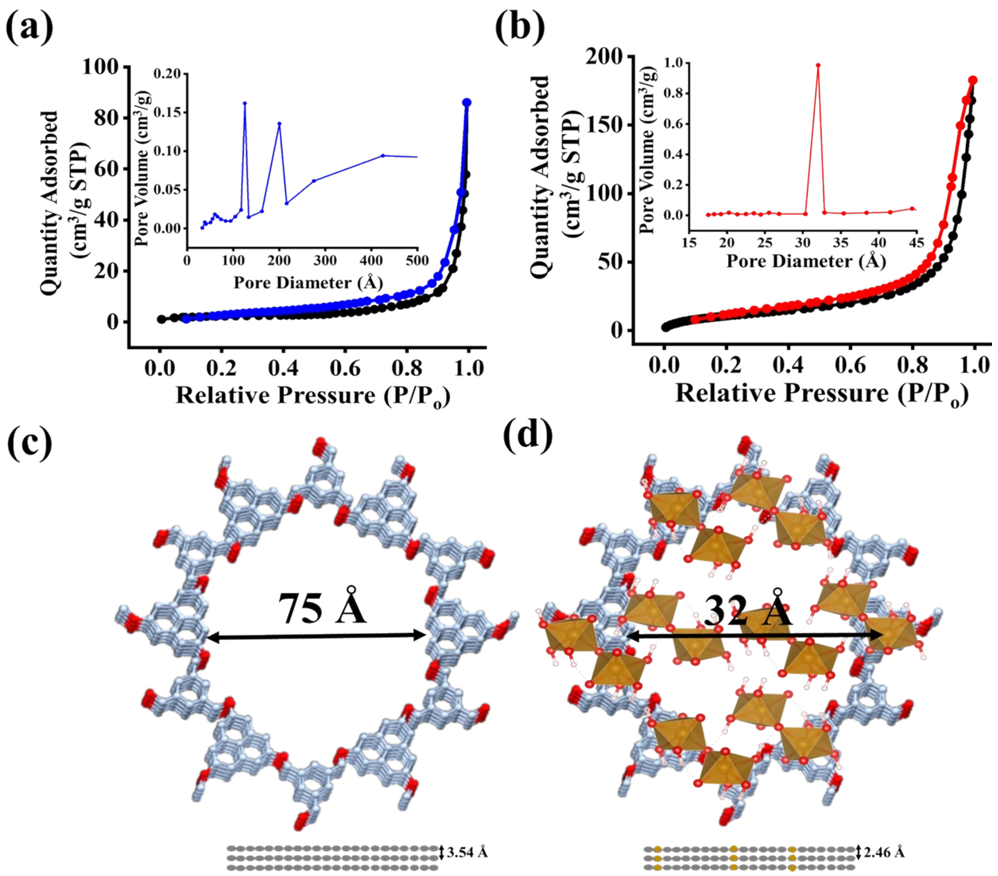

Figure 10. Nitrogen adsorption-desorption isotherms of (a) Btc/M and (b) Btc/M-FeOOH, and 3D pore structure illustrations of (c) Btc/M and (d) Btc/M-FeOOH.

12. BET Surface Area and t-Plot Analysis of Btc/M and Btc/M-FeOOH

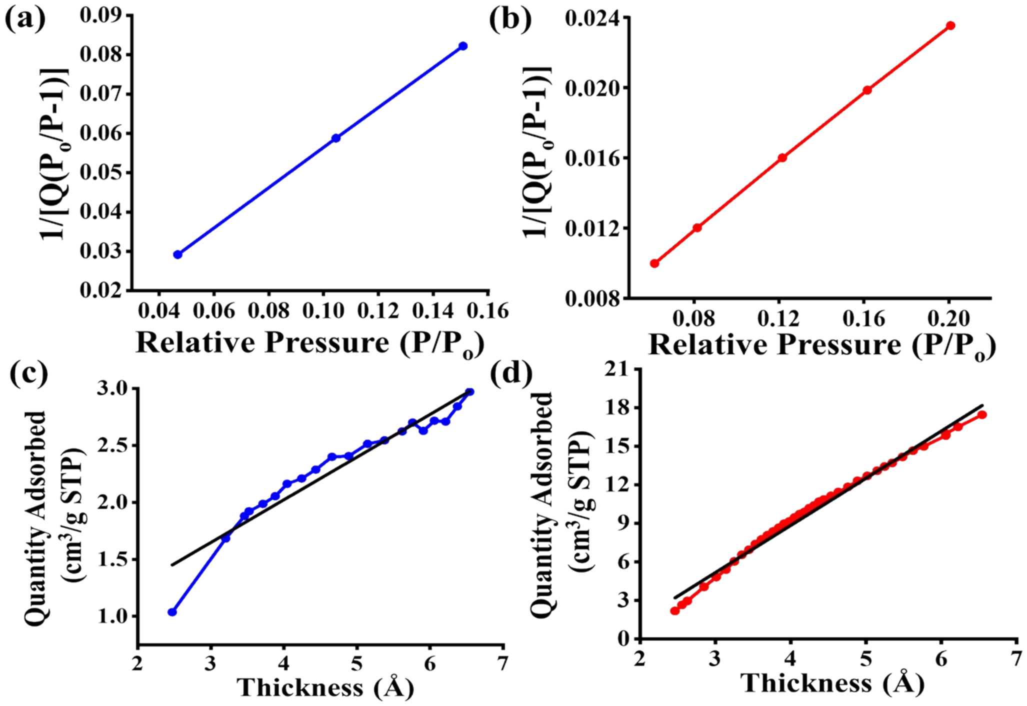

Figure S11. Surface area plot of (a) Btc/M (blue) and (b) Btc/M-FeOOH (red), and t-plot of Btc/M (blue) and Btc/M-FeOOH (red).

13. Thermal Stability Analyses: Raman Spectroscopy, Differential Scanning Calorimetry (DSC), and Thermogravimetric (TGA)

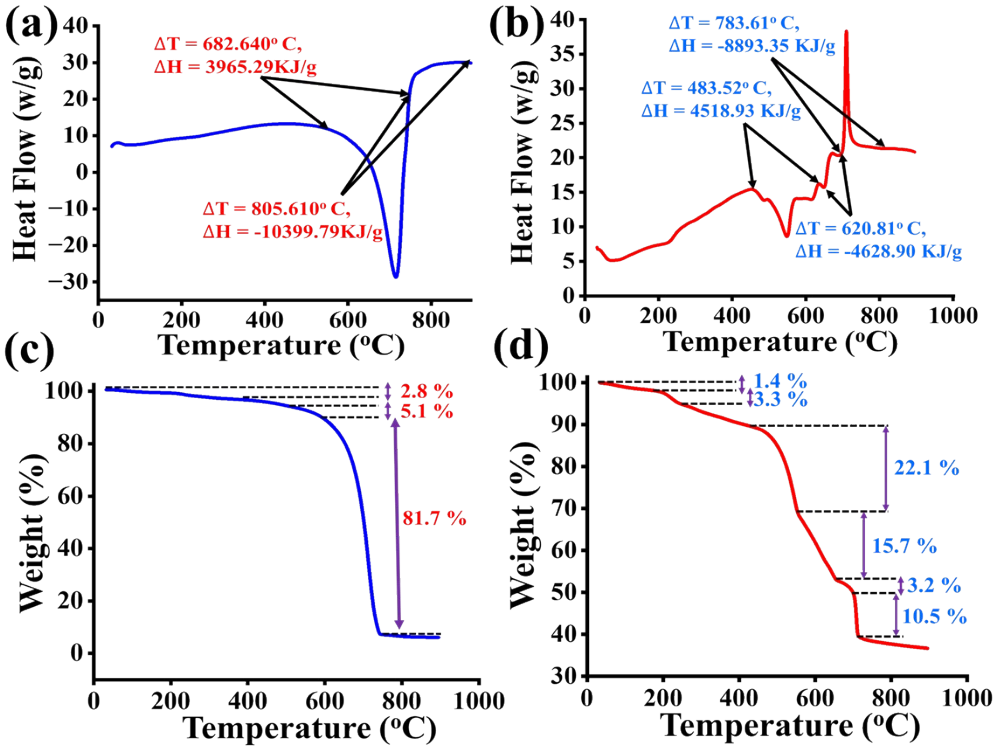

Figure S12. Differential scanning calorimetry (DSC) curve of (a) Btc/M and (b) Btc/M-FeOOH, and Thermogravimetric curve of (c) Btc/M and (d) Btc/M-FeOOH.

14. Morphological Architecture and Elemental Distribution from Electron Microscopy

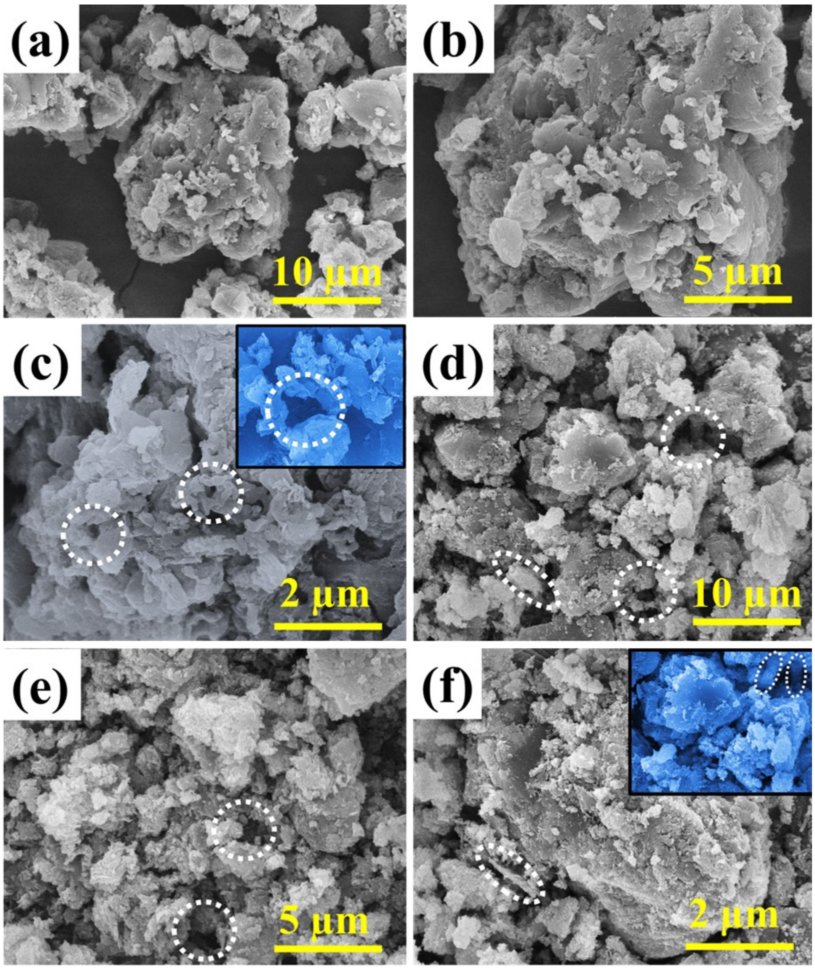

Figure S13. Field emission scanning electron microscopy (FE-SEM) micrographs of Btc/M (a-c), and Btc/M-FeOOH (d-f).

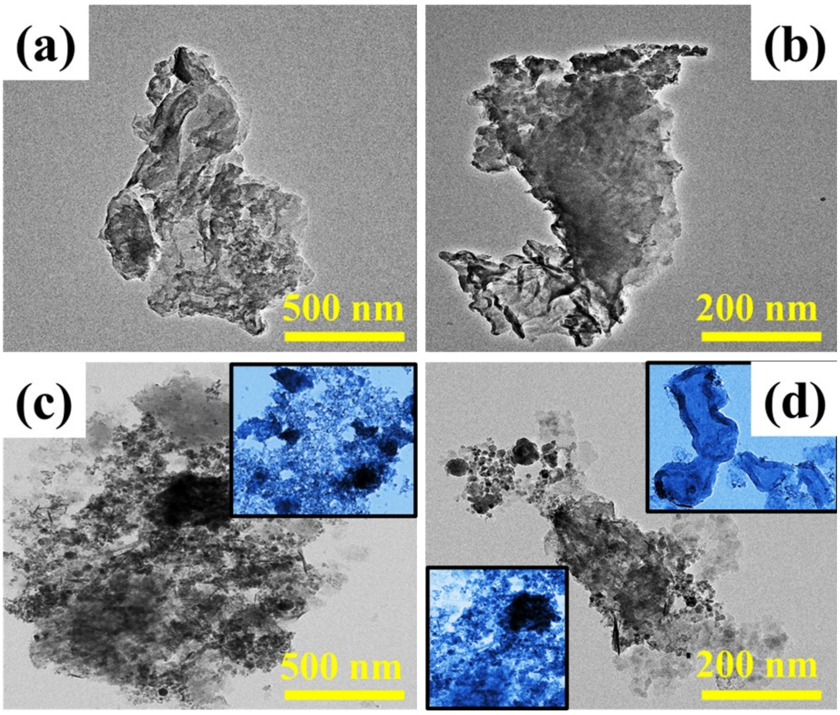

Figure S14. Transmission electron microscopy (TEM) images of Btc/M (a-b), and Btc/M-FeOOH (c-d).

15. UV-vis spectroscopy and Fourier Transform Infrared Spectroscopy of precursors

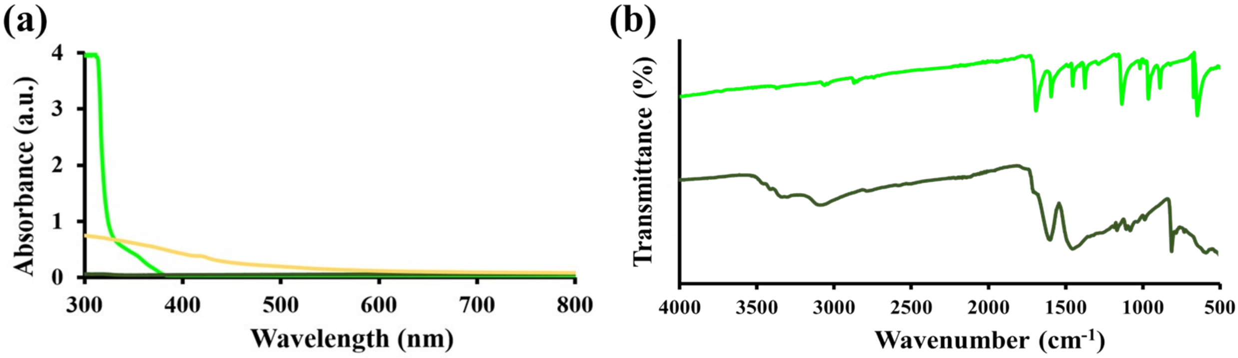

Figure S15. (a) UV-vis spectra of Btc (light green), M (dark green), and FeOOH nanorods (yellow), and (b) FTIR spectra of Btc (light green) and M (dark green).

16. Cyclic Voltammetry (CV), Electrochemical Impedance Spectroscopy (EIS), Tafel Plot, and Chronopotentiometry (CP) of precursors

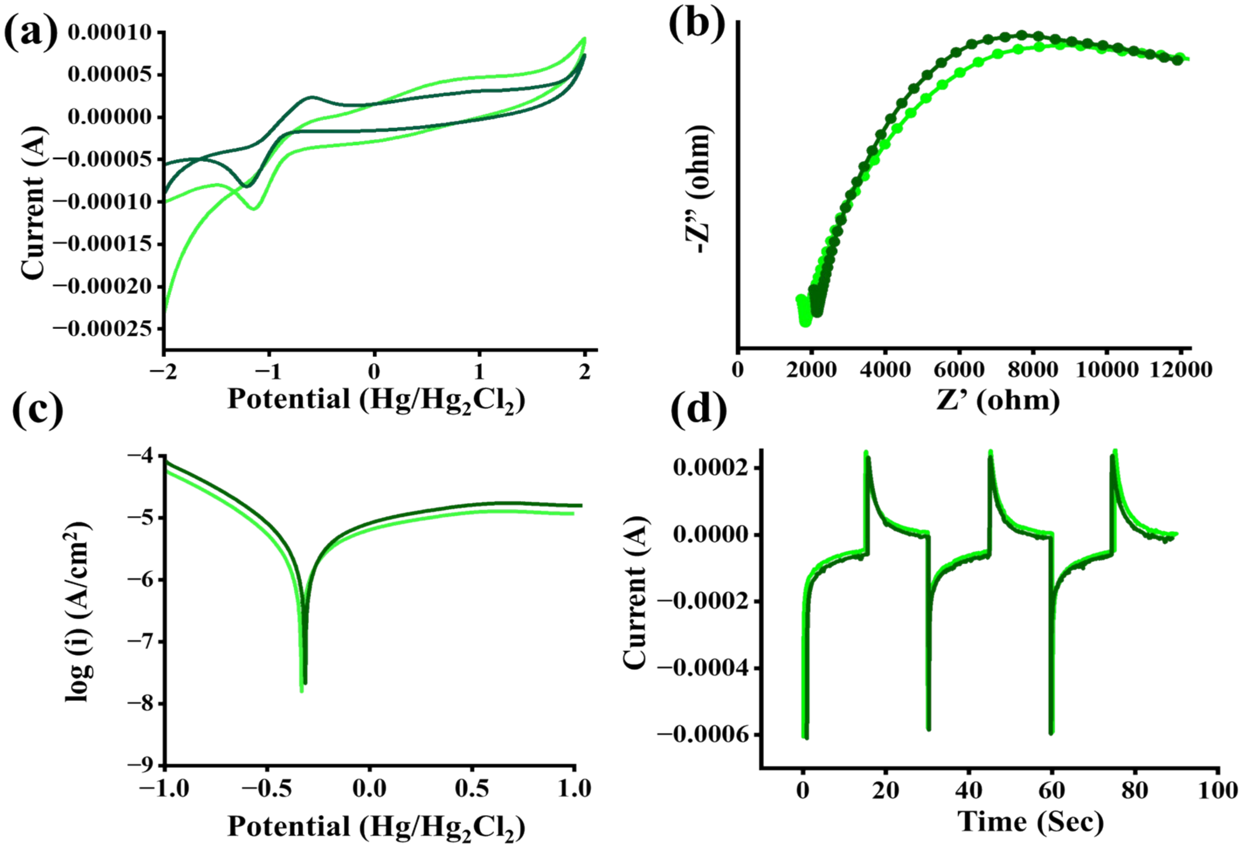

Figure S16. (a) CV of Btc (light green) and M (dark green), (b) EIS of of Btc (light green) and M (dark green), (c) Tafel plot of Btc (light green) and M (dark green), and (d) CP of Btc (light green) and M (dark green).

17. Visible-Light-Mediated Hydroxylation of Boronic Acids

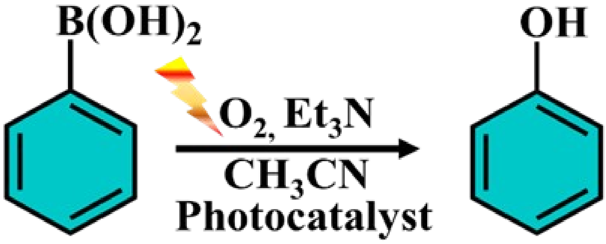

Figure S17. Photocatalytic conversion of boronic acids to phenols.

18. Plausible mechanistic pathway for boronic acid conversion

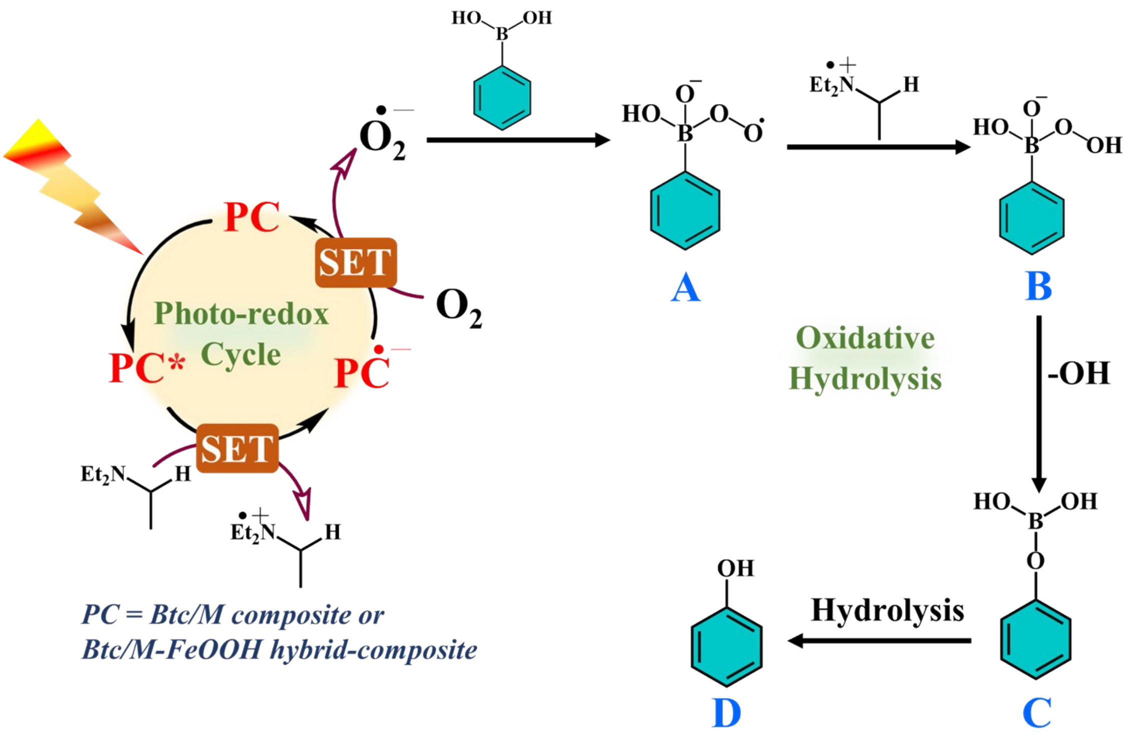

Figure S18. Plausible mechanistic pathway for boronic acid conversion.

19. UV-vis. spectra of synthesized organic products

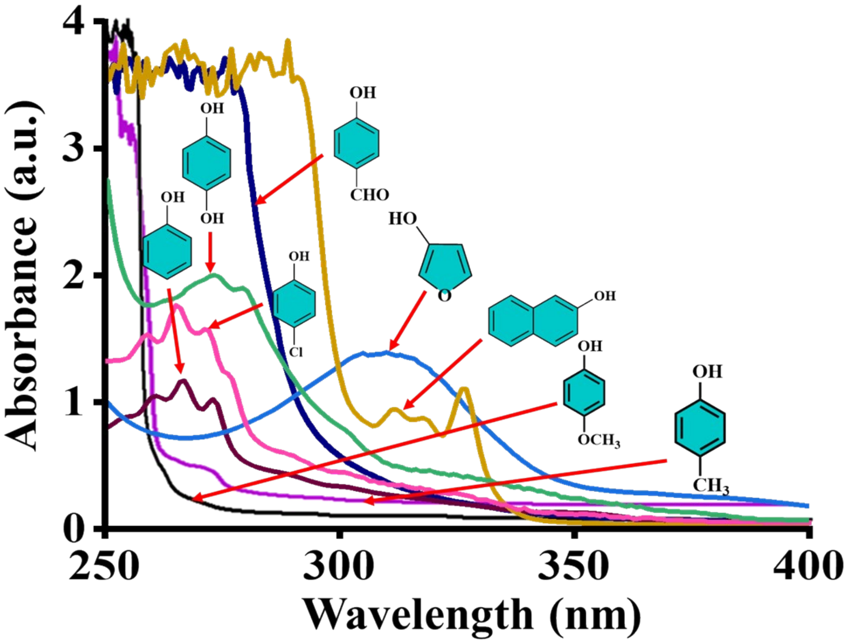

Figure S19. UV-vis. spectra of organic products.

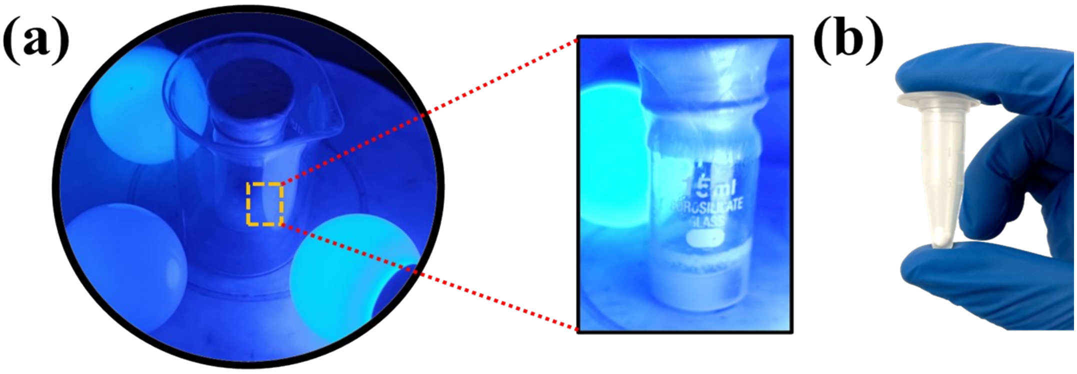

Figure S20. Photographs of the (a) experimental setups and (b) product of boronic acid conversion.

20. Optimization table for boronic acid conversions

Entry[a]	Catalyst	Light Source	Catalyst Loading (mg)	Et_3N (mmol)	Time (h)	Yield [b]
1.	**Btc/M**	**Blue LED**	**5**	**0.3**	**24**	**97.4**
2.	**Btc/M-FeOOH**	**Blue LED**	**5**	**0.3**	**24**	**98.1**
3.	**Btc/M-FeOOH**	**Blue LED**	**2**	**0.3**	**24**	**82.3**
4.	**Btc/M-FeOOH**	**Blue LED**	**5**	**1**	**24**	**93.8**
5.	**Btc/M-FeOOH**	**Blue LED**	**5**	**-**	**24**	**10.3**
6.	**Btc/M-FeOOH**	**Blue LED**	**1**	**0.3**	**24**	**65.4**
7.	**Btc/M-FeOOH**	**-**	**5**	**0.3**	**24**	**2.8**
8.	**Btc/M**	**White LED**	**5**	**0.3**	**24**	**70.1**
9.	**Btc/M-FeOOH**	**White LED**	**5**	**0.3**	**24**	**74.5**

Table S1: Optimization by varying moles of catalyst and base. [a] Reaction conditions: phenylboronic acid (0.1 mmol), photocatalyst (2 mg), Et_3N (0.3 mmol), 5 mL CH_3CN, O_2, 24 h, blue LED (25W), [b] Isolated yield.

21. Strategies for the Regeneration of 1,4-NADH

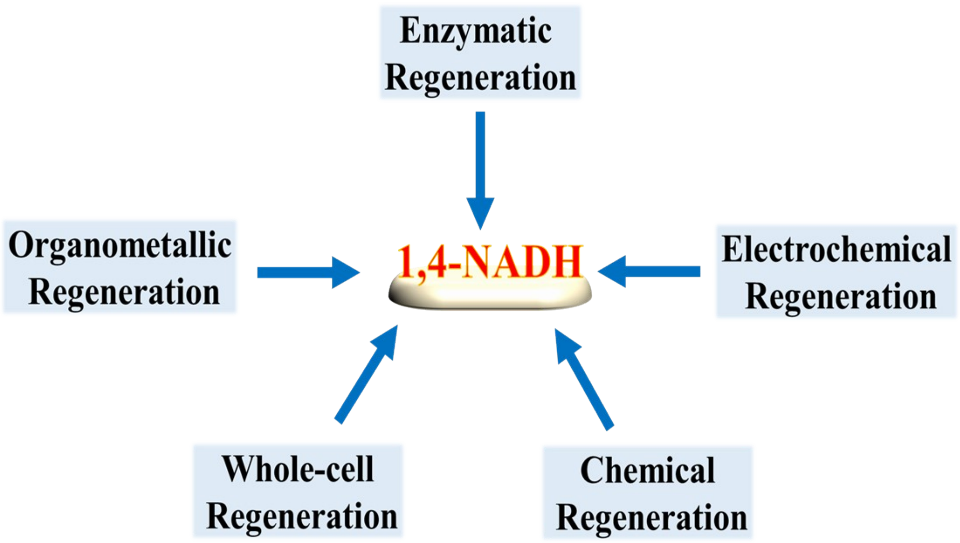

Figure S21. Strategies for the Regeneration of 1,4-NADH.

22. Future scopes of NADH

S.no.	Enzymes	Substrate(s)	By-Product(s)	Advantages
1.	Alcohol Dehydrogenase (ADH)	Benzaldehyde (or other oxidizable aldehydes)	Benzyl Alcohol (or other respective alcohol)	High activity, low cost[4]
2.	Formate Dehydrogenase (FDH)	Carbon Dioxide (CO_2)	Formic Acid	Reduces greenhouse gases towards green and sustainable technologies.[5]
3.	Glutamate Dehydrogenase (GDH)	Alpha-Ketoglutaric acid	Glutamic Acid	Enables nitrogen assimilation and cellular function.[6]
4.	Formaldehyde Dehydrogenase (F_{ald}DH) + FDH + ADH	Carbon Dioxide (CO_2)	Methanol	Supports green chemical industry development.[7]
5.	-	Carbon Dioxide (CO_2) + Benzyl Amine	Formic Acid	Provides a stable, low-cost, and scalable method without enzyme-related limitations.[8]
6.	Nitrogenase	N_2	Ammonia	Aids food

				production, stores hydrogen, serves as fuel, and supports green industry.[9]
7.	Aldehyde Dehydrogenase (ALDH)	Formaldehyde	Formic Acid	Waste-water detoxification (aldehyde removal).[10]

Table S2: Future scopes of NADH for different photocatalytic applications.

23. Plausible mechanistic pathway for 1,4-NADH regeneration using Co-C/Rh-C electron mediators

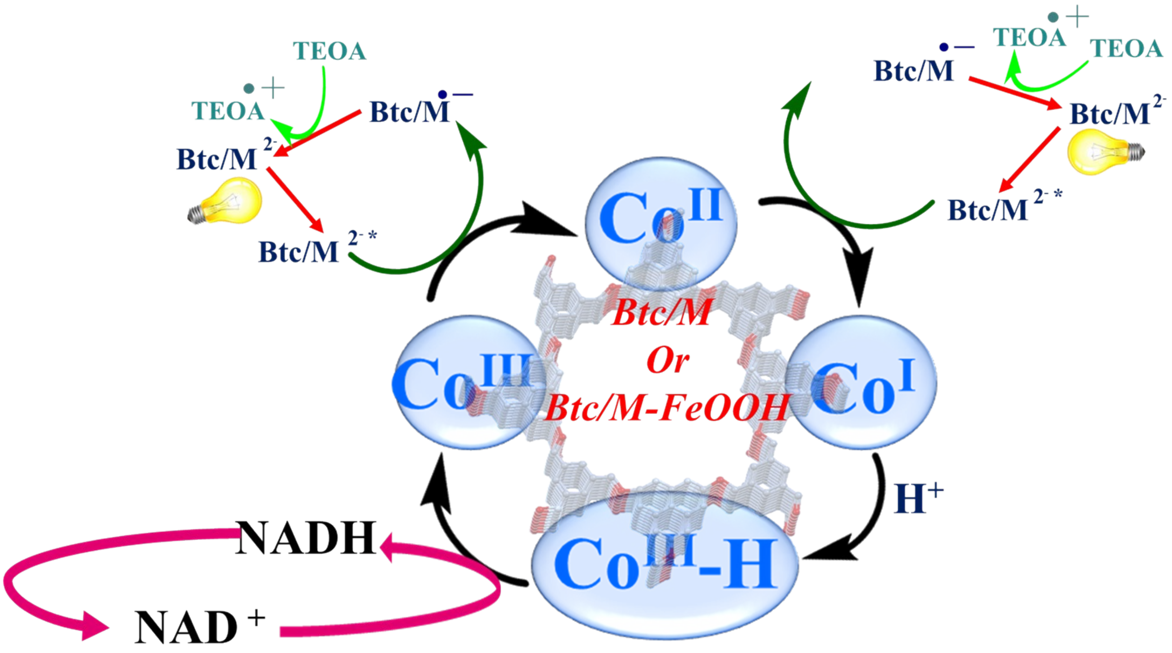

Figure S22. Plausible mechanistic pathway via Co-C.

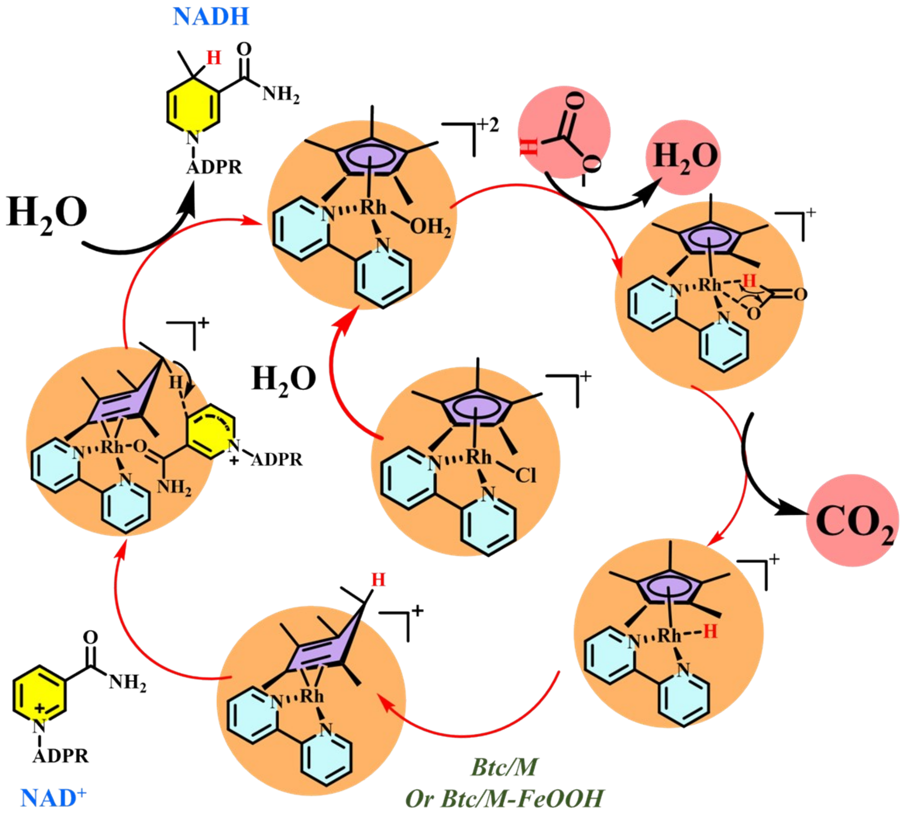

Figure S23. Plausible mechanistic pathway via Rh-C.

24. UV-vis. spectra of the NADH experiment

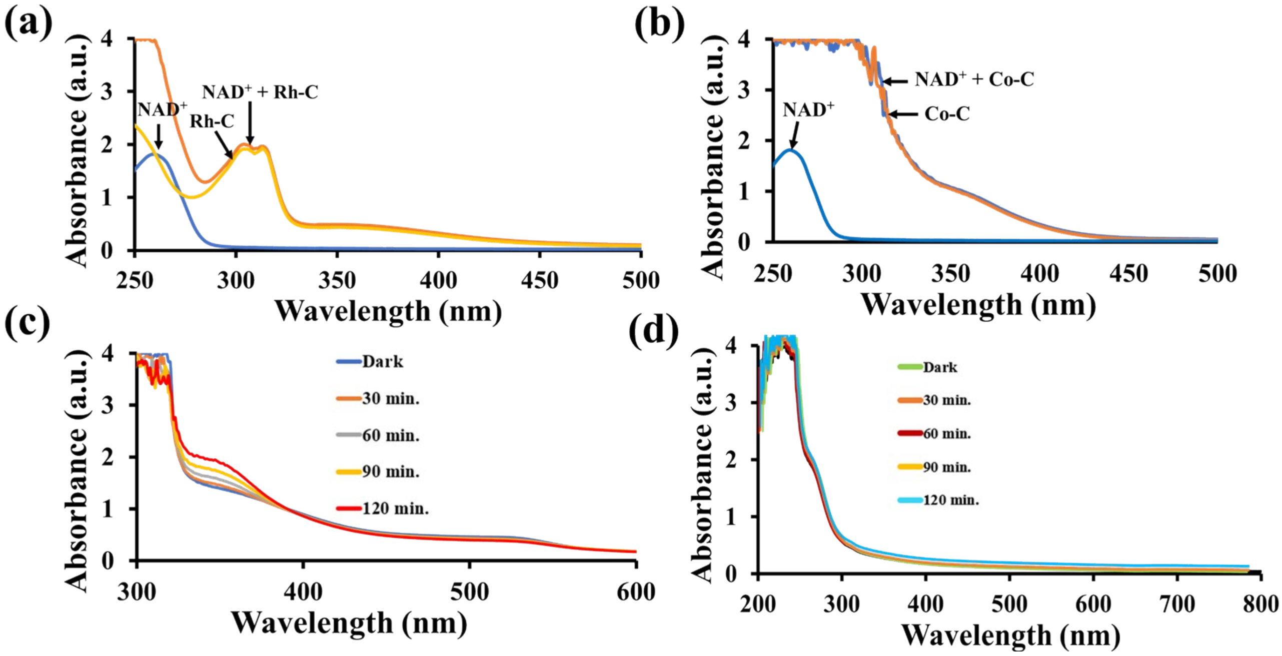

Figure S24. UV-vis. spectra of (a) Rh-C mediated cycle, (b) Co-C mediated cycle, NADH photo-regeneration via (c) Btc/M (Rh-C mediated), and (d) Btc/M-FeOOH (Co-C mediated).

25. Optimization table for photo-regeneration of NADH

Entry	Catalyst	Electron Mediator	Light Source	TEOA (M)	NAD^+ (mM)	pH	1,4-NADH Yield (%)
1.	Btc/M	Co-C	Blue LED	4	5	7	35.58
2.	Btc/M	Rh-C	Blue LED	4	5	7	62.37
3.	Btc/M-FeOOH	Co-C	Blue LED	4	5	7	78.18
4.	Btc/M-FeOOH	Rh-C	Blue LED	4	5	7	95.49
5.	Btc/M	Rh-C	Blue LED	2	5	7	Less 20%
6.	Btc/M-FeOOH	Rh-C	Blue LED	2	5	7	Less 20%
7.	Btc/M	Co-C	Blue LED	1	5	7	Less 25%
8.	Btc/M-FeOOH	Co-C	Blue LED	1	5	7	Less 25%
9.	-	Co-C/Rh-C	Blue LED	4	5	7	N.D.
10.	Btc/M-FeOOH	-	Blue LED	4	5	7	N.D.
11.	Btc/M-FeOOH	Co-C/Rh-C	Blue LED	-	5	7	N.D.
12.	Btc/M-FeOOH	Co-C/Rh-C	-	4	5	7	N.D.
13.	Btc/M-FeOOH	Co-C/Rh-C	Blue LED	4	-	7	N.D.
14.	Btc/M-FeOOH	Co-C/Rh-C	Blue LED	4	5	10	45
15.	Btc/M-FeOOH	Co-C/Rh-C	Blue LED	4	5	5	10
16.	Btc	Co-C/Rh-C	Blue LED	4	5	7	< 5
17.	M	Co-C/Rh-C	Blue LED	4	5	7	< 10
18.	FeOOH	Co-C/Rh-C	Blue LED	4	5	7	N.D.

Table S3: Optimization by varying reaction conditions for photo-regeneration of NADH.

Entry	**Photocatalyst**	**NADH % Yield**
1.	**Fe-aminoclay/g-C_3N_4 heterojunction**	**71.24**[11]
2.	**g-C_3N_4 engineered with aniline / $K_3[Fe(CN)_6]$**	**71.80**[12]
3.	**Cp*Rh-implanted conjugated microporous polymer (DTS/Rh@CMP-1)**	**33.00**[13]
4.	**Gold nanocapsules (Au NCPs)**	**22.65**[14]

Entry[a]	**Photocatalyst**	**Electron Mediator**	**Turnover Number (TON)**	**Time (h)**	**Turnover Frequency (TOF) (h^{-1})**
1.	**Btc/M**	**Co-C**	**1.37**	**2**	**0.68**
2.	**Btc/M**	**Rh-C**	**2.06**	**2**	**1.03**
3.	**Btc/M-FeOOH**	**Co-C**	**2.08**	**2**	**1.04**
4.	**Btc/M-FeOOH**	**Rh-C**	**2.11**	**2**	**1.05**
5.	**Btc**	**Co-C**	**-**	**2**	**-**
6.	**Btc**	**Rh-C**	**-**	**2**	**-**
7.	**M**	**Co-C**	**-**	**2**	**-**
8.	**M**	**Rh-C**	**-**	**2**	**-**
9.	**FeOOH**	**Co-C**	**-**	**2**	**-**
10.	**FeOOH**	**Rh-C**	**-**	**2**	**-**

Table S4: Optimization of TON and TOF for photo-regeneration of NADH. [a] Reaction conditions: NAD^+ (5 mM), TEOA (4 M), Rh-C/Co-C complex (5 mM), and the photocatalyst (1 mM; either Btc/M or Btc/M-FeOOH) in phosphate-buffered solution (PBS, 100 mM, pH 7.0).

5.	**MIL-125-NH₂ MOF (Rh-metalated)**	**66.40**[15]
6.	**TCPP immobilized on thiolated SiO_2, coated with PDA/PEI**	**9.64% (no Rh mediator** **22.5% (with Rh mediator)**[16]
7.	**Rh-implanted conjugated microporous polymer (Rh@CMP-1)**	**33.00**[13]
8.	**Btc/M COF**	**62.37** **(Rh-C mediated)** **35.58** **(Co-C mediated)** ***(This Work)***
9.	**Btc/M-FeOOH MOF**	**95.49** **(Rh-C mediated)** **78.18** **(Co-C mediated)** ***(This Work)***

Table S5: Comparison of NADH regeneration efficiencies achieved by different photocatalysts from recent literature with the present Btc/M and Btc/M-FeOOH systems.

26. Reusability result via PXRD

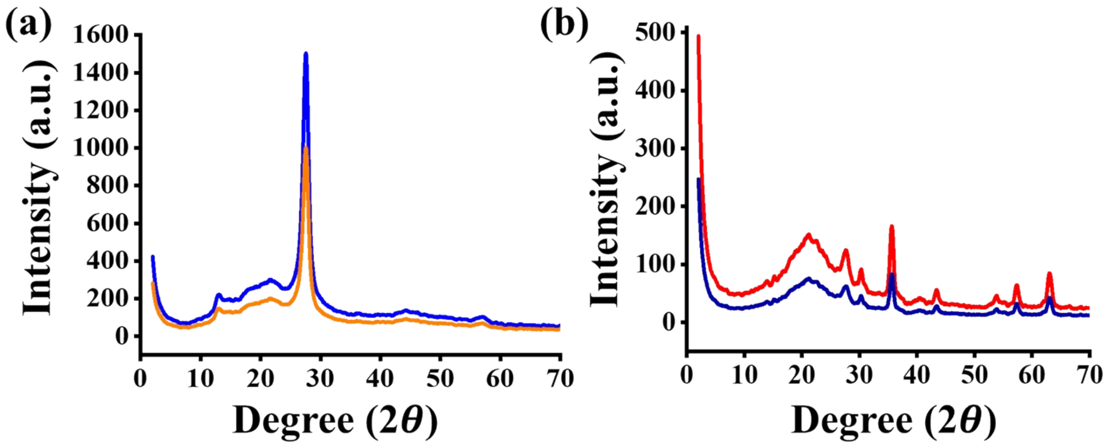

Figure S25. PXRD pattern of post-reaction after five consecutive cycles (a) fresh Btc/M (red) and recovered Btc/M (blue), and (b) fresh Btc/M-FeOOH (blue) and recovered Btc/M-FeOOH.

27. Schematic representation of the present work

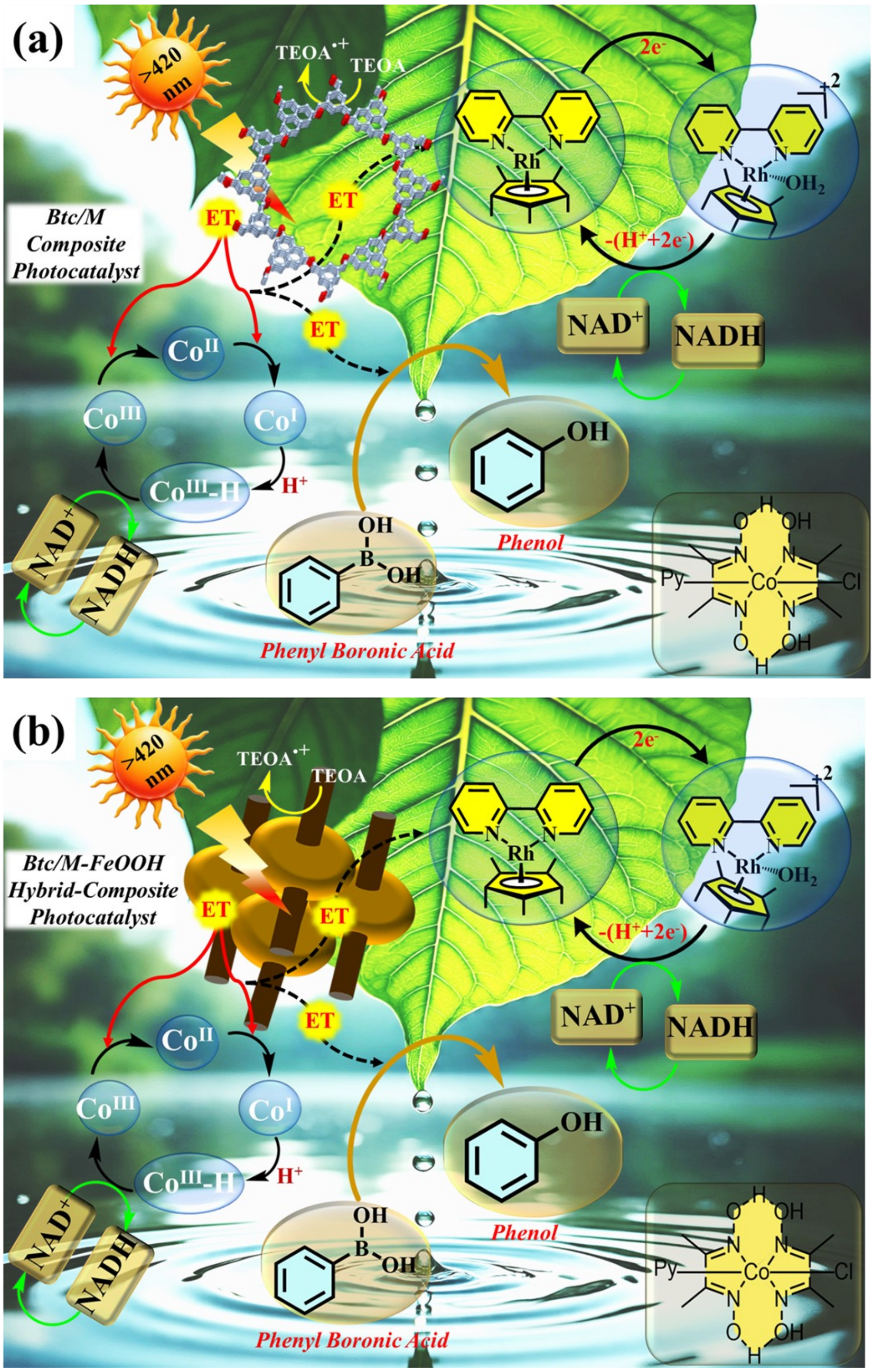

Scheme S1. Schematic representation showing photo-regeneration and boronic acid hydroxylation via (a) Btc/M and (b) Btc/M-FeOOH.

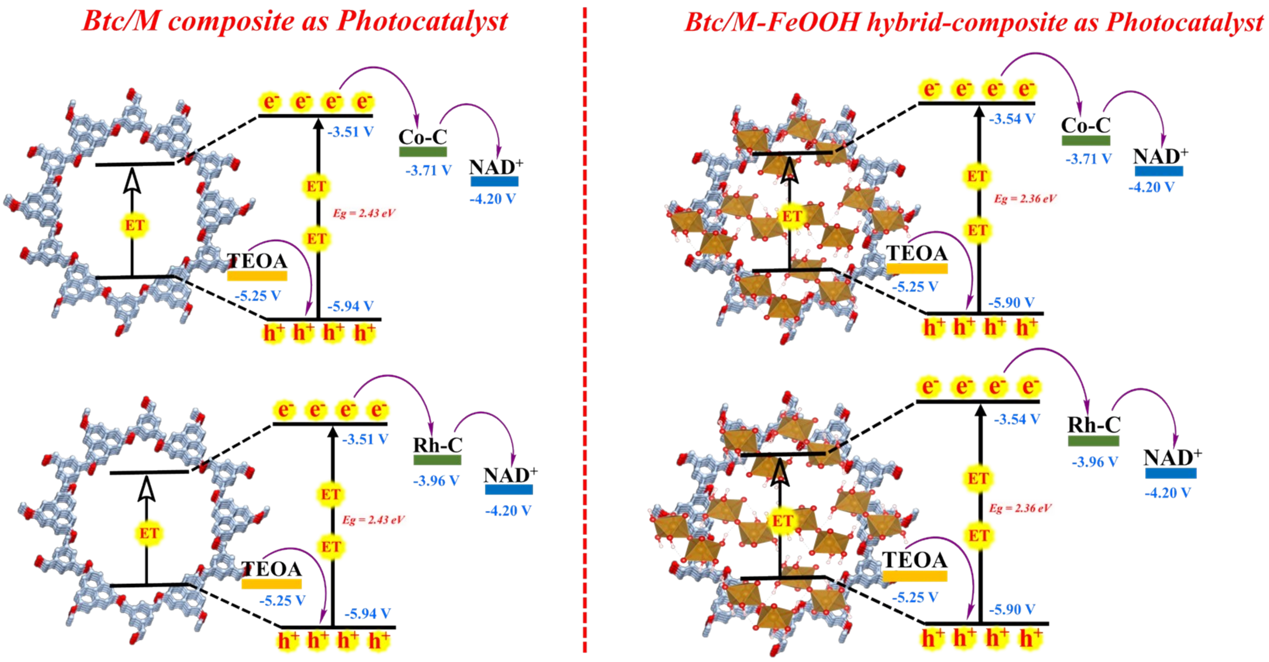

Scheme S2. Schematic illustration of the energy flow diagram for photo-regeneration of 1,4-NADH from Btc/M and Btc/M-FeOOH.

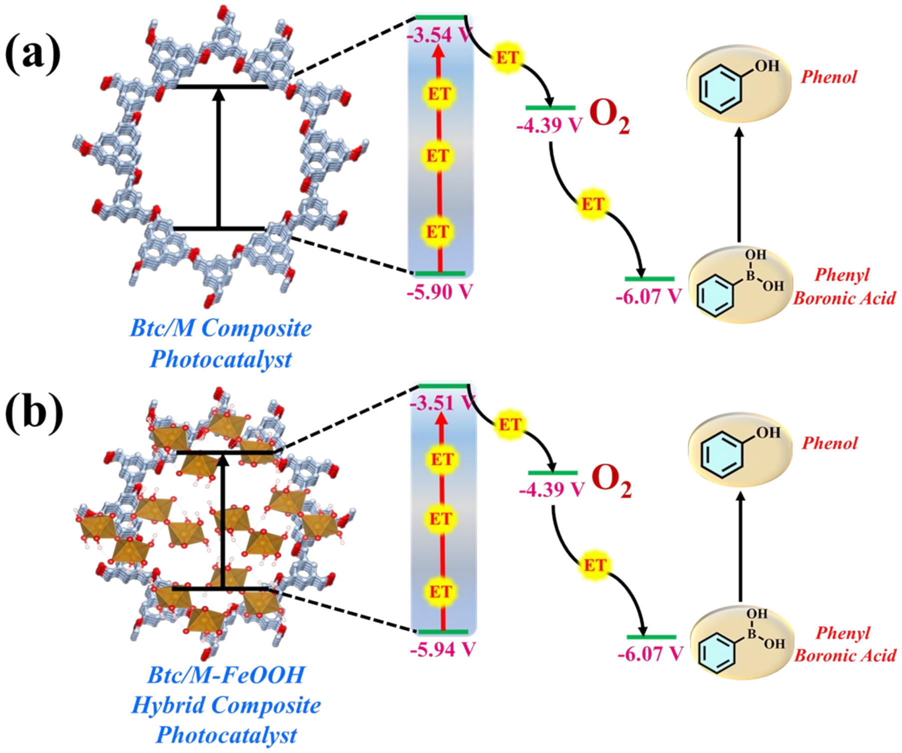

Scheme S3. Energy flow diagram of boronic acid hydroxylation via alignment of redox potentials.

28. NMR spectra

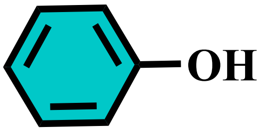

(a) Phenol: White solid, ^{1}H NMR (500 MHz, $CDCl_3$) δ 7.51-7.53 (m,2H), 7.35-7.41 (m,2H), 7.14-7.17 (t,1H, J=10 Hz), 5.61 (s,1H).

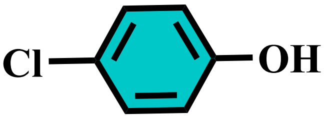

(b) 4-Chlorophenol: White solid, ^{1}H NMR (500 MHz, $CDCl_3$) δ 7.46 (d,2H, J=5 Hz), 7.37 (d,2H, J=5 Hz), 4.81 (s,1H).

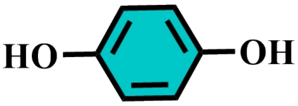

(c) Hydroquinone: White solid, ^{1}H NMR (500 MHz, DMSO-d6) δ 7.69 (s,4H), 6.48 (s,2H).

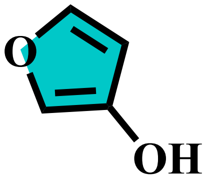

(d) 3-Furanol: White solid, ^{1}H NMR (500 MHz, DMSO-d6) δ 7.87 (d,1H, J= 5Hz), 7.79 (s,1H), 7.58 (d,1H, J= 5Hz), 6.48 (s,1H).

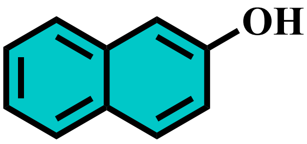

(e) 2-Naphthol: White solid, ^{1}H NMR (500 MHz, DMSO-d6) δ 7.69-7.72 (t,2H, J= 5Hz), 7.61-7.63 (d,1H, J = 10Hz), 7.44-7.50 (m,2H), 7.32-7.35 (m,1H), 7.19-7.22 (ddd,1H, J = 5Hz), 5.03 (s,1H).

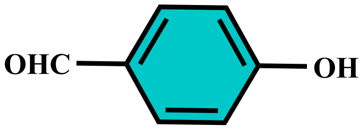

(f) 4-hydroxybenzaldehyde: White solid, ^{1}H NMR (500 MHz, DMSO-d6) δ 10.03 (s, 1H), δ 8.31 (s, 1H), δ 7.97-7.98 (d, 2H, J = 5 Hz), δ 7.87-7.85 (d, 2H, J = 10 Hz).

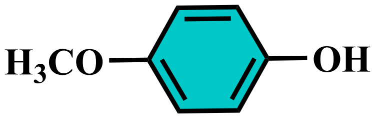

(g) 4-methoxyphenol: Off white solid, ^{1}H NMR (500 MHz, $CDCl_3$) δ 8.49 (s, 1H), 6.95-6.93 (d, 2H, J = 10Hz), 6.85-6.83 (d, 2H, J = 10Hz), 3.76 (s, 3H).

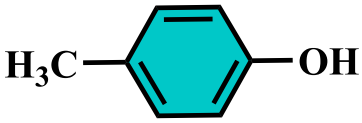

(h) p-cresol: Brown solid, ^{1}H NMR (500 MHz, $CDCl_3$) δ 8.50 (s, 1H), 6.95-6.93 (d, 2H, J = 10Hz), 6.69-6.67 (d, 2H, J = 10Hz), 2.56 (s, 3H).

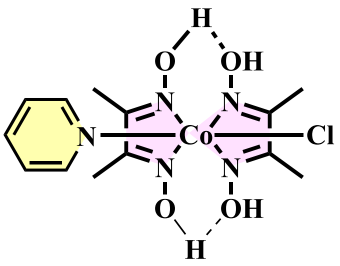

(i) Co-C: Brown solid, ^{1}H NMR (500 MHz, $CDCl_3$) δ 8.24 (d,2H, J = 5 Hz), 7.69 (t,1H), 7.21(d,2H, J = 5 Hz), 5.28 (s,4H), 2.37 (s,12H)

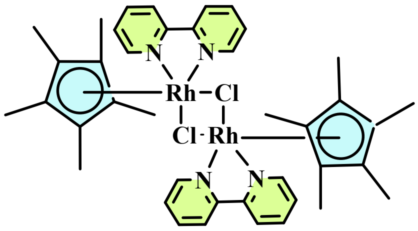

(j) Rh-C: Orange solid, ^1H NMR (500 MHz, $CDCl_3$) δ 9.02 (d,1H, J = 5 Hz), 8.86 (dd,1H), 8.30 (dd,1H), 7.80 (d,1H, J = 5 Hz), 1.78 (s,7H), 1.28 (s,1H)

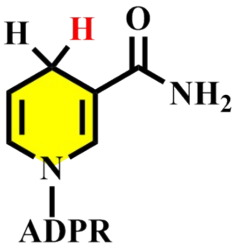

(k) 1,4-NADH: In the reaction medium, ^1H NMR (500 MHz, D_2O) δ for 1,4-NADH at 6.55 arises due to hydrogen atoms on the pyridine ring (solvation effect)[17]**.**

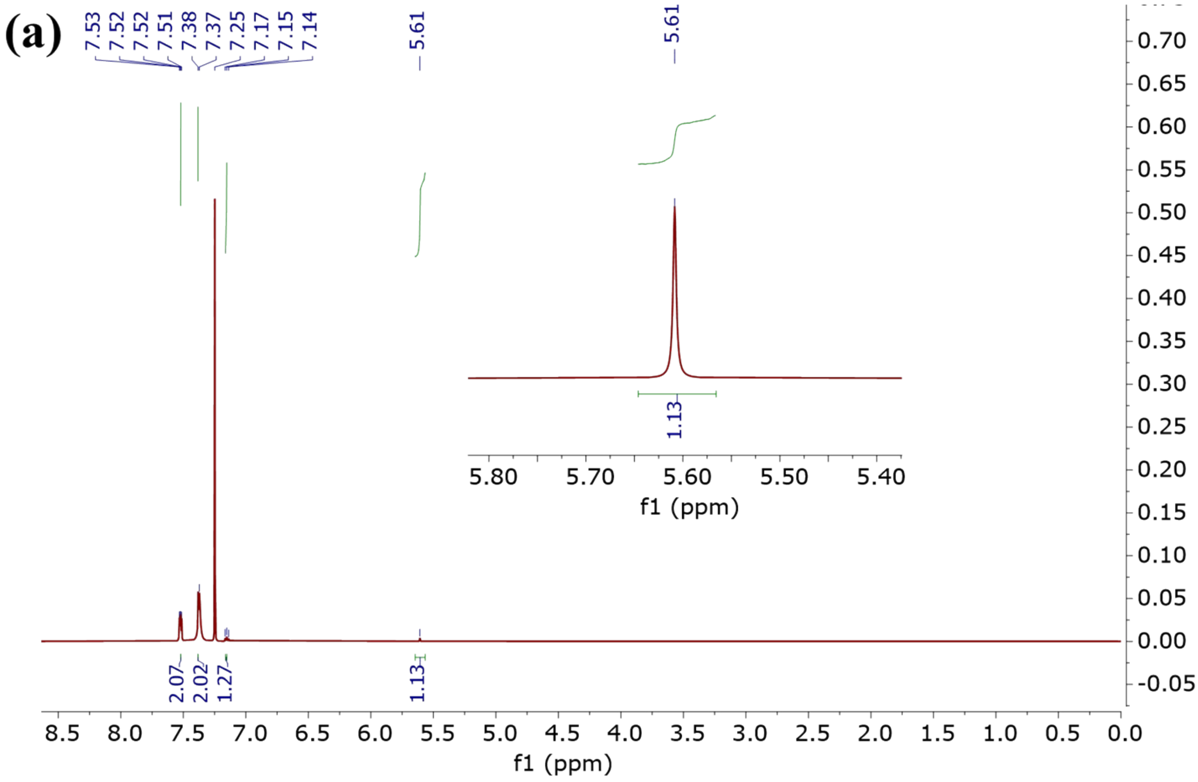

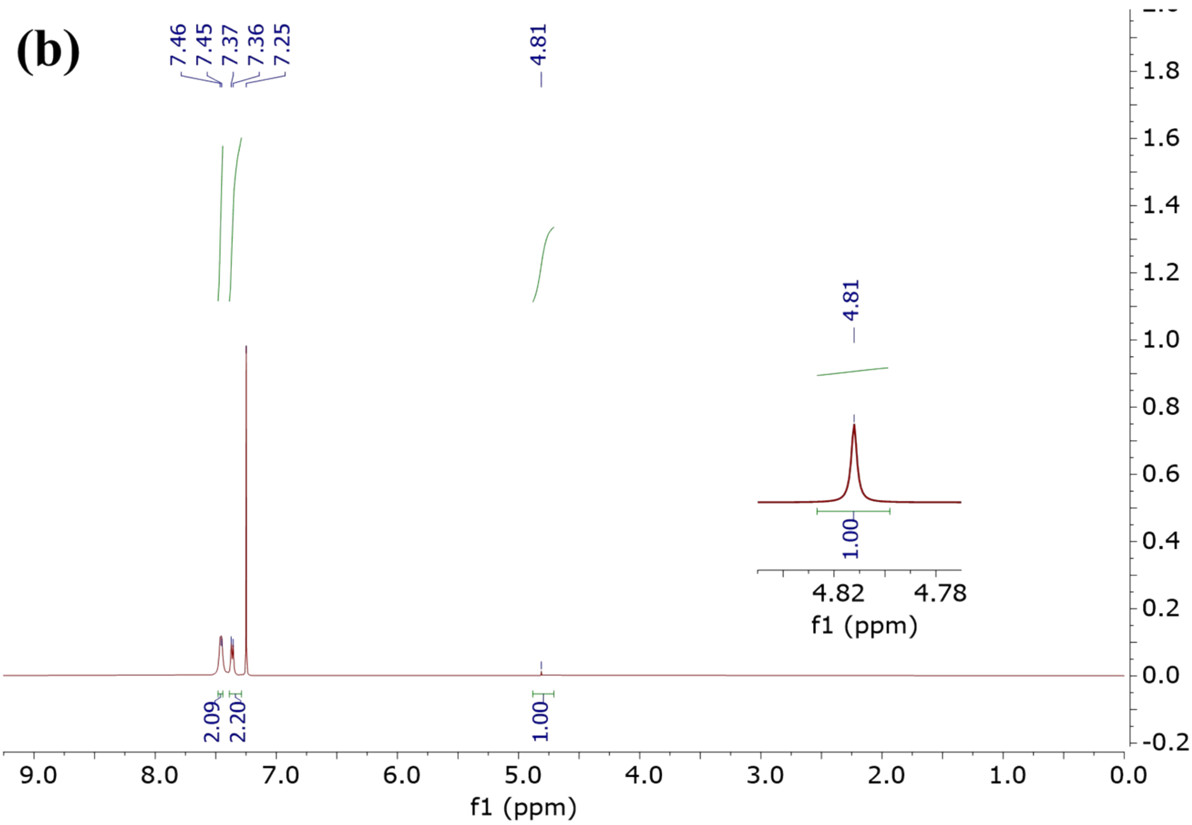
(b)
7.46
7.45
7.37
7.36
7.25
4.81
2.09
2.20
1.00
4.81
1.00
4.82
4.78
f1 (ppm)
1.8
1.6
1.4
1.2
1.0
0.8
0.6
0.4
0.2
0.0
-0.2
9.0
8.0
7.0
6.0
5.0
4.0
3.0
2.0
1.0
0.0
f1 (ppm)

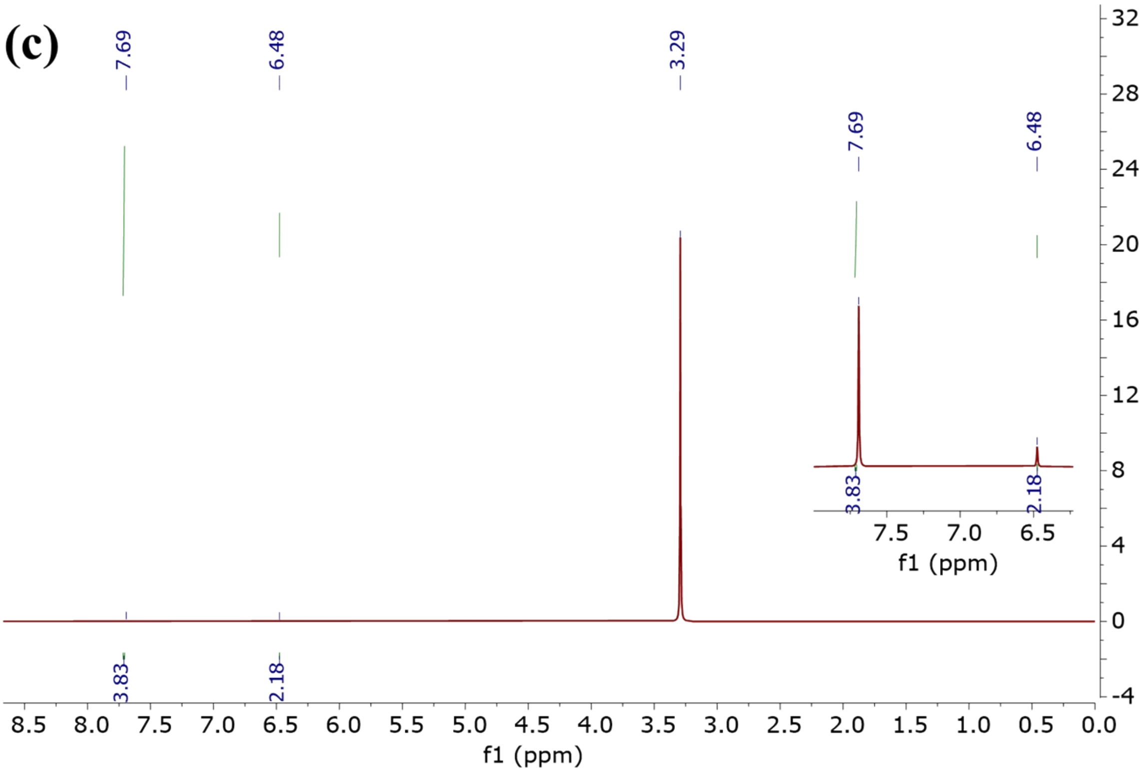
(c)
7.69
6.48
3.29
7.69
6.48
3.83
2.18
7.5
7.0
6.5
f1 (ppm)
3.83
2.18
32
28
24
20
16
12
8
4
0
-4
8.5
8.0
7.5
7.0
6.5
6.0
5.5
5.0
4.5
4.0
3.5
3.0
2.5
2.0
1.5
1.0
0.5
0.0
f1 (ppm)

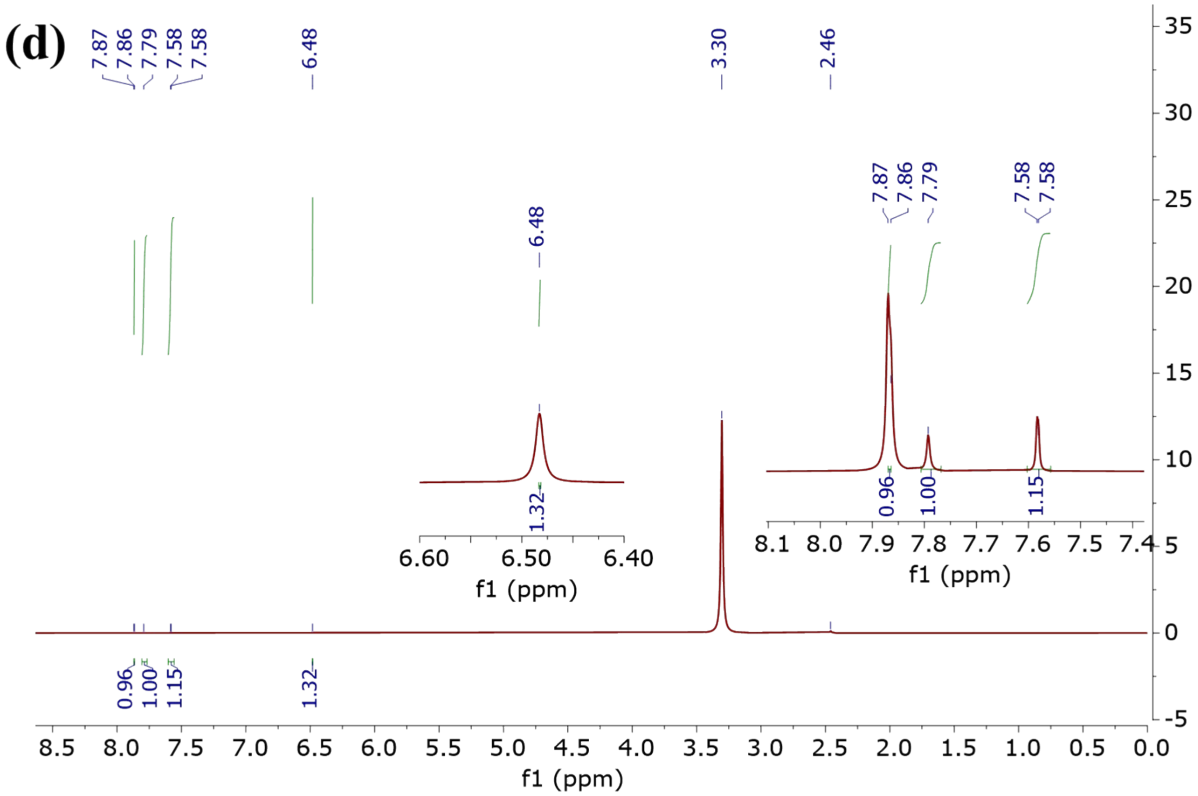
(d)
7.87
7.86
7.79
7.58
7.58
6.48
3.30
2.46
0.96
1.00
1.15
1.32
6.60
6.50
6.40
f1 (ppm)
8.1
8.0
7.9
7.8
7.7
7.6
7.5
7.4
35
30
25
20
15
10
5
0
-5
8.5
8.0
7.5
7.0
6.5
6.0
5.5
5.0
4.5
4.0
3.5
3.0
2.5
2.0
1.5
1.0
0.5
0.0
f1 (ppm)

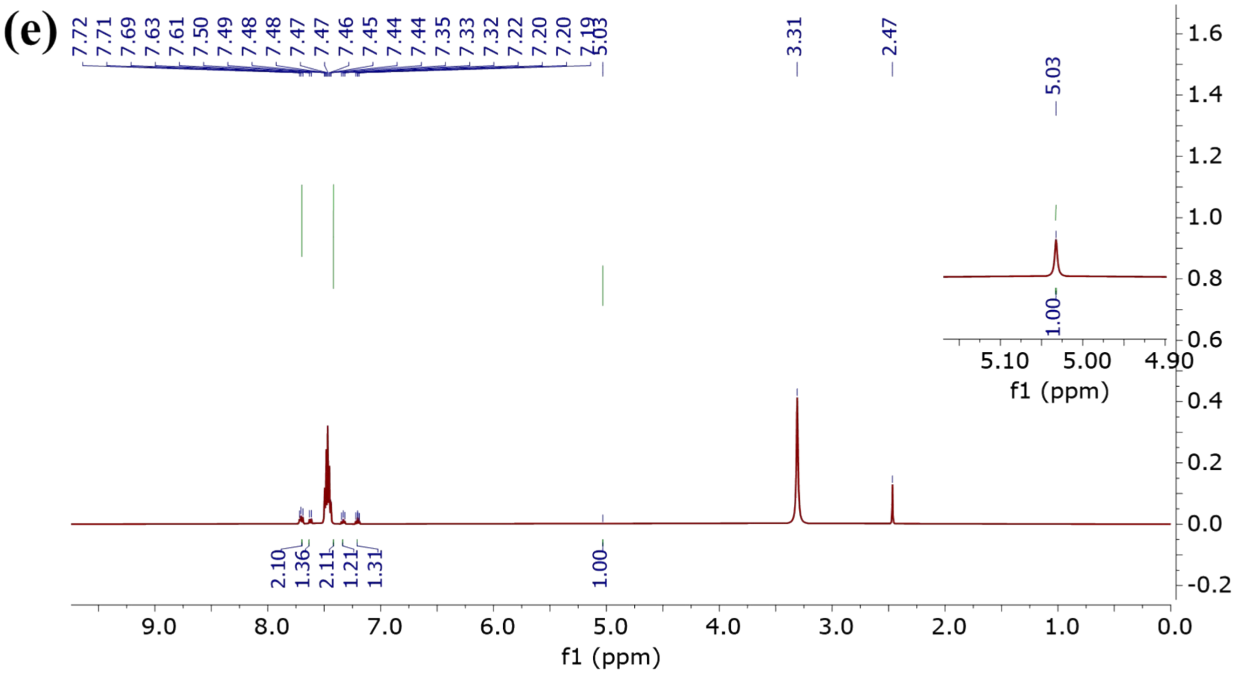
(e)
7.72
7.71
7.69
7.63
7.61
7.50
7.49
7.48
7.48
7.47
7.47
7.46
7.45
7.44
7.44
7.35
7.33
7.32
7.22
7.20
7.20
7.19
5.03
3.31
2.47
5.03
1.00
5.10
5.00
4.90
f1 (ppm)
2.10
1.36
2.11
1.21
1.31
1.00
1.6
1.4
1.2
1.0
0.8
0.6
0.4
0.2
0.0
-0.2
9.0
8.0
7.0
6.0
5.0
4.0
3.0
2.0
1.0
0.0
f1 (ppm)

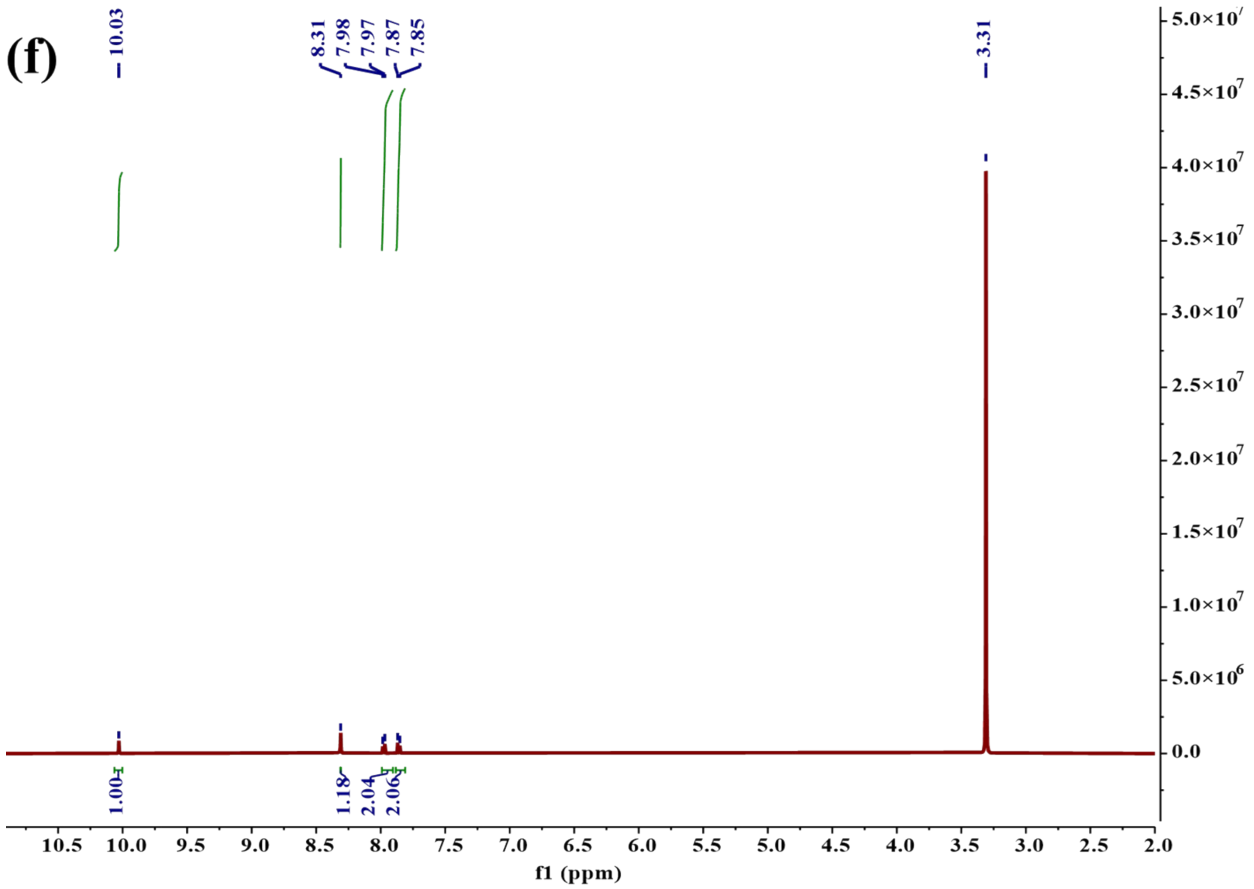
(f)
10.03
8.31
7.98
7.97
7.87
7.85
3.31
1.00
1.18
2.04
2.06
5.0×10⁷
4.5×10⁷
4.0×10⁷
3.5×10⁷
3.0×10⁷
2.5×10⁷
2.0×10⁷
1.5×10⁷
1.0×10⁷
5.0×10⁶
0.0
10.5
10.0
9.5
9.0
8.5
8.0
7.5
7.0
6.5
6.0
5.5
5.0
4.5
4.0
3.5
3.0
2.5
2.0
f1 (ppm)

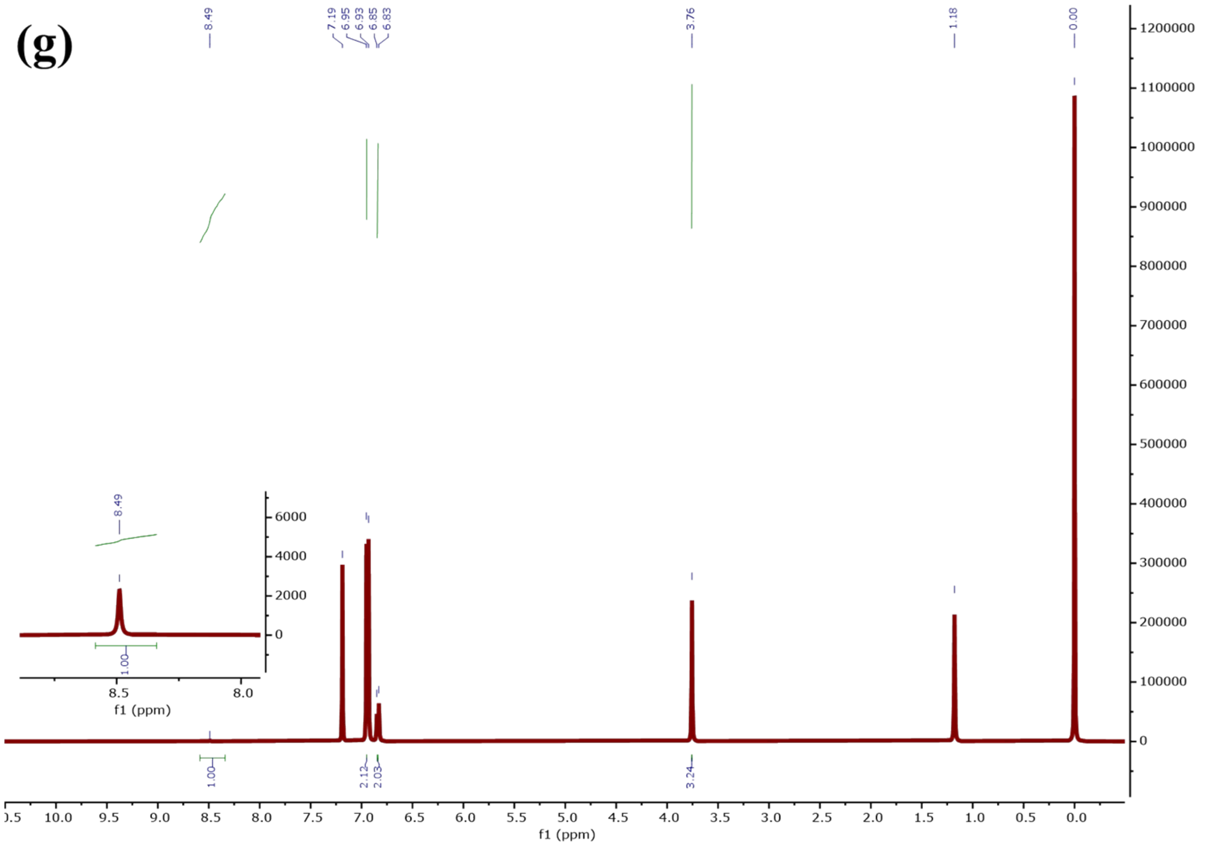
(g)
8.49
7.19
6.95
6.93
6.85
6.83
3.76
1.18
0.00
1200000
1100000
1000000
900000
800000
700000
600000
500000
400000
300000
200000
100000
0
6000
4000
2000
0
8.49
1.00
8.5
8.0
f1 (ppm)
1.00
2.12
2.03
3.24
10.5
10.0
9.5
9.0
8.5
8.0
7.5
7.0
6.5
6.0
5.5
5.0
4.5
4.0
3.5
3.0
2.5
2.0
1.5
1.0
0.5
0.0
f1 (ppm)

(h)

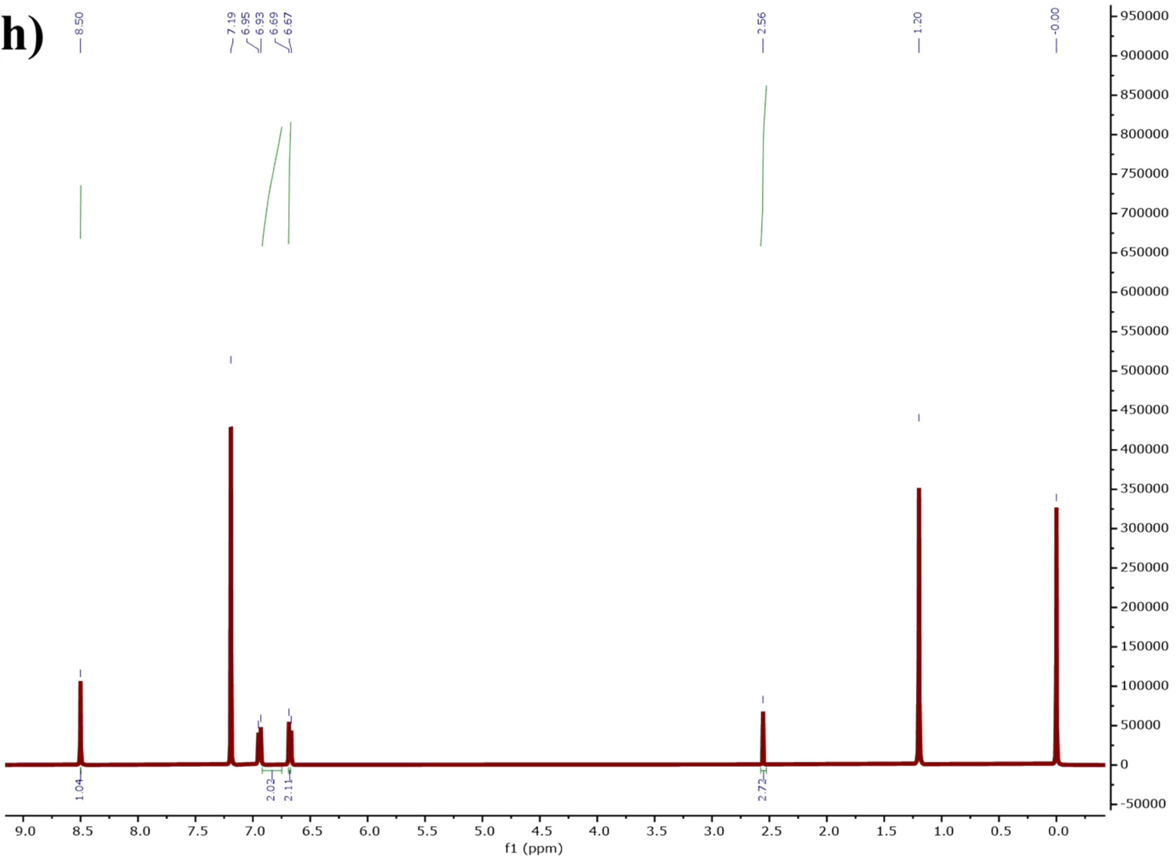
8.50
7.19
6.95
6.93
6.69
6.67
2.56
1.20
-0.00
1.04
2.02
2.11
2.72
950000
900000
850000
800000
750000
700000
650000
600000
550000
500000
450000
400000
350000
300000
250000
200000
150000
100000
50000
0
-50000
9.0
8.5
8.0
7.5
7.0
6.5
6.0
5.5
5.0
4.5
4.0
3.5
3.0
2.5
2.0
1.5
1.0
0.5
0.0
f1 (ppm)

(i)

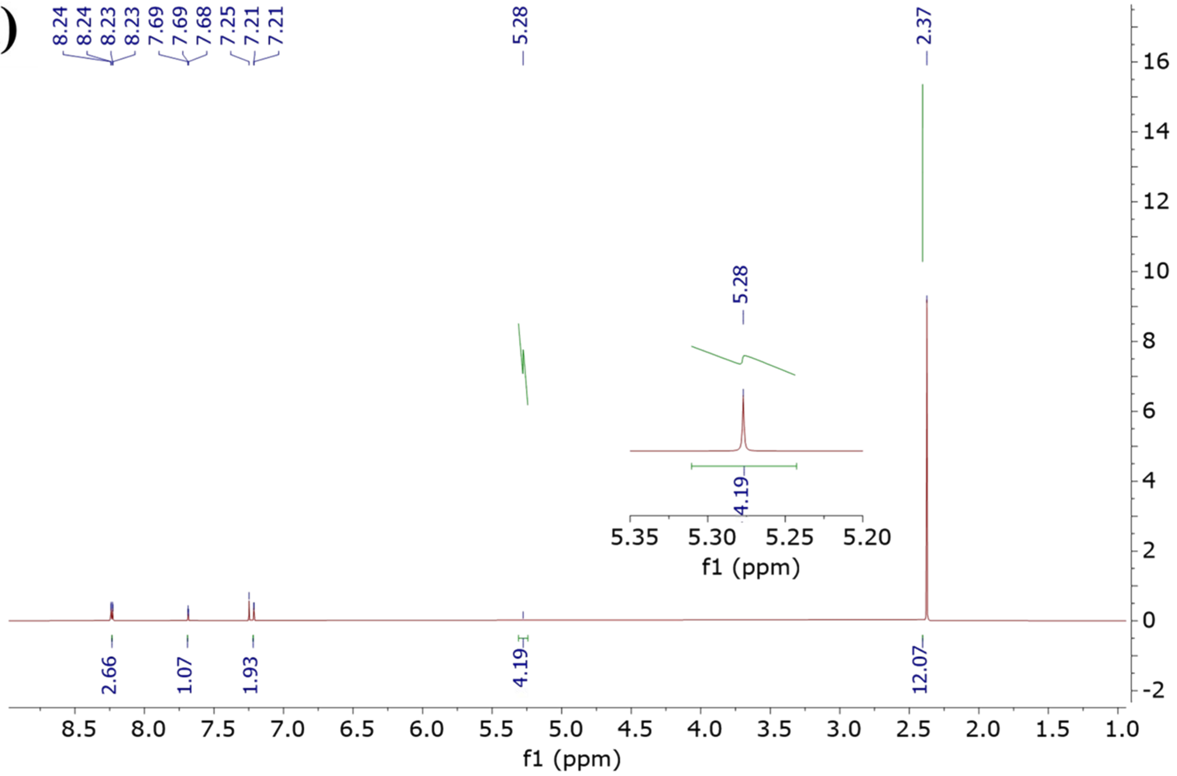
8.24
8.24
8.23
8.23
7.69
7.69
7.68
7.25
7.21
7.21
5.28
2.37
5.28
4.19
5.35
5.30
5.25
5.20
f1 (ppm)
2.66
1.07
1.93
4.19
12.07
16
14
12
10
8
6
4
2
0
-2
8.5
8.0
7.5
7.0
6.5
6.0
5.5
5.0
4.5
4.0
3.5
3.0
2.5
2.0
1.5
1.0
f1 (ppm)

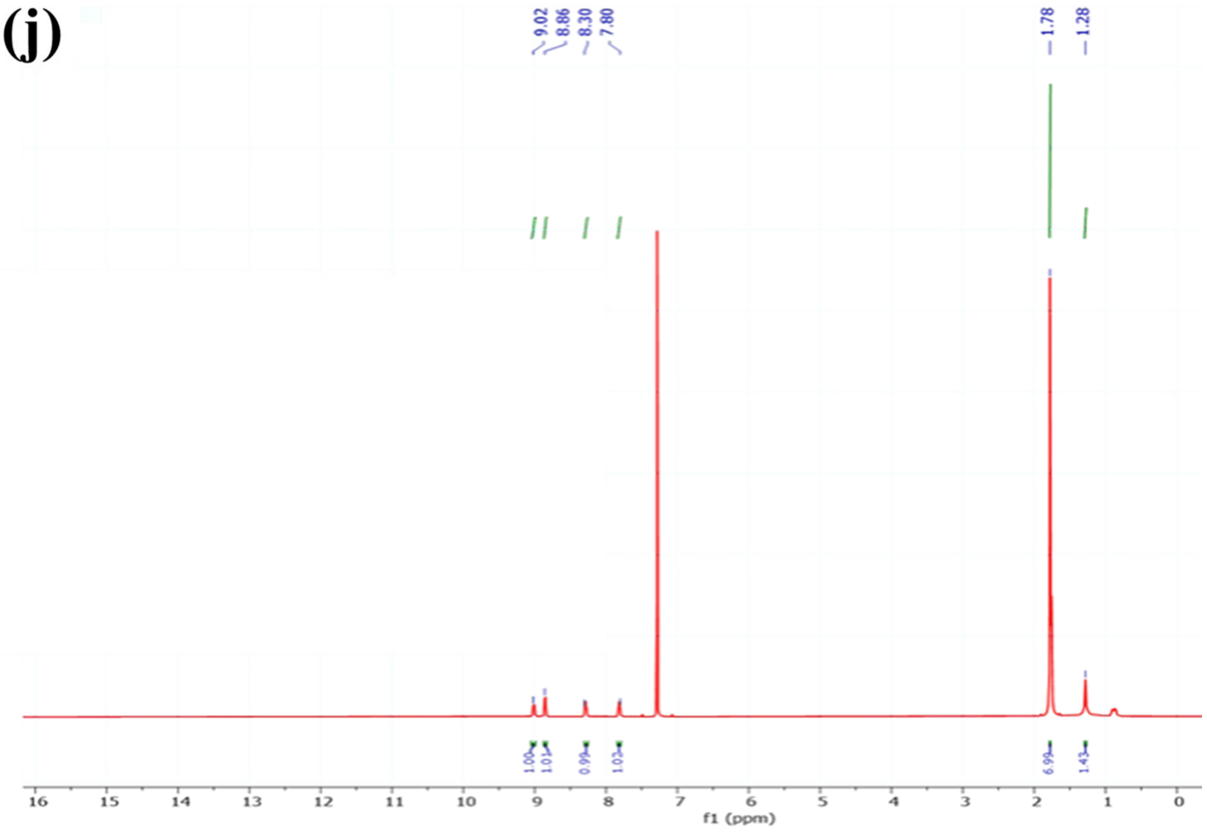
(j)
9.02
8.86
8.30
7.80
1.78
1.28
1.00
1.01
0.99
1.03
6.99
1.43
16
15
14
13
12
11
10
9
8
7
6
5
4
3
2
1
0
f1 (ppm)

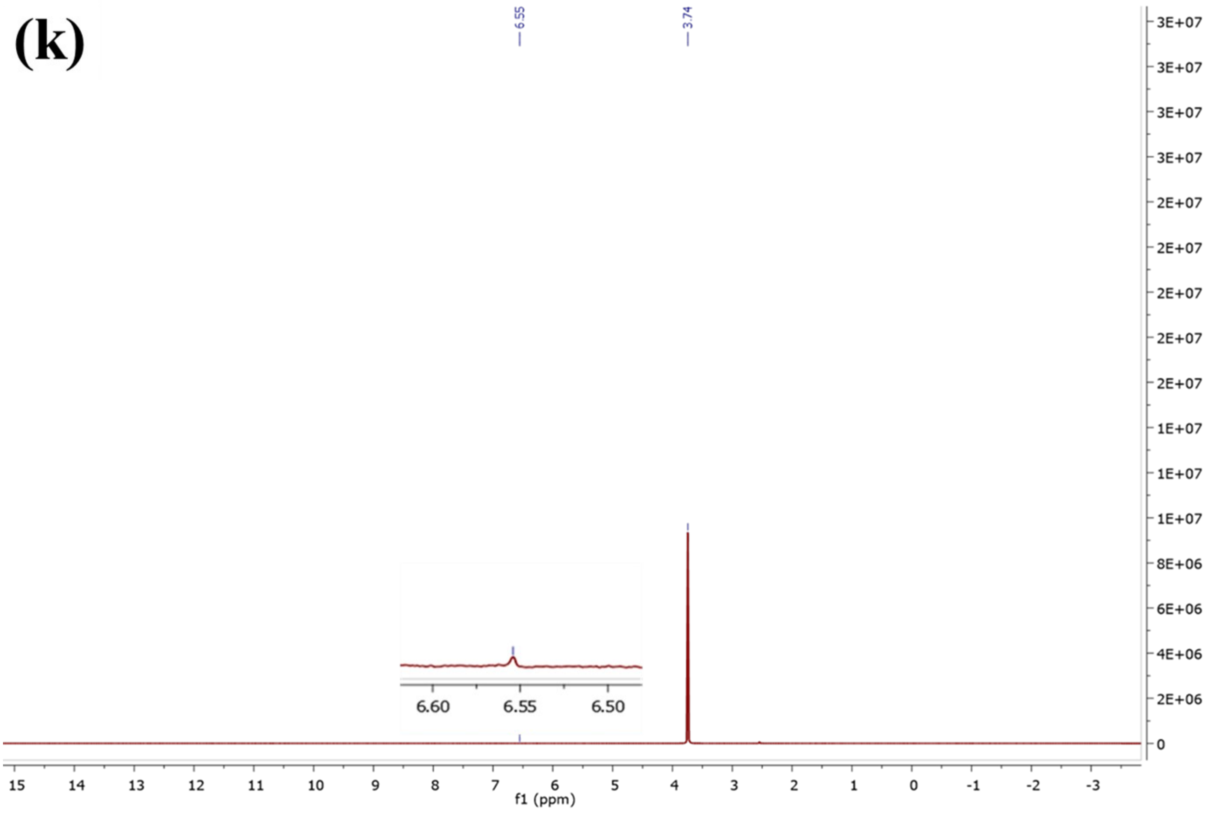
(k)
6.55
3.74
3E+07
3E+07
3E+07
3E+07
2E+07
2E+07
2E+07
2E+07
2E+07
1E+07
1E+07
1E+07
8E+06
6E+06
4E+06
2E+06
0
6.60
6.55
6.50
15
14
13
12
11
10
9
8
7
6
5
4
3
2
1
0
-1
-2
-3
f1 (ppm)

29. References

1 J. A. Kim, S. Kim, J. Lee, J. O. Baeg and J. Kim, *Inorg. Chem.*, 2012, **51**, 8057–8063.

2 S. Mishra, R. K. Yadav, R. Shahin, K. Sharma and J. O. K. Baeg, *Diam. Relat. Mater.*, 2025, **158**, 112604.

3 S. Betanzos-Lara, Z. Liu, A. Habtemariam, A. M. Pizarro, B. Qamar and P. J. Sadler, *Angew. Chemie*, 2012, **124**, 3963–3966.

4 S. Servi, D. Tessaro and G. Pedrocchi-Fantoni, *Coord. Chem. Rev.*, 2008, **252**, 715–726.

5 T. Hartmann and S. Leimkühler, *FEBS J.*, 2013, **280**, 6083–6096.

6 H. Wang, Y. Chen, X. Hou, C. Ma and T. Tan, *Green Chem.*, 2016, **18**, 3250–3256.

7 G.-Y. Xu, J.-H. Guo, Y.-C. Qu, Y. Zhang, Y. Fu and Q.-X. Guo, *Green Chem.*, 2016, **18**, 5510–5517.

8 W.-H. Wang, Y. Himeda, J. T. Muckerman, G. F. Manbeck and E. Fujita, *Chem. Rev.*, 2015, **115**, 12936–12973.

9 B. M. Hoffman, D. Lukoyanov, Z.-Y. Yang, D. R. Dean and L. C. Seefeldt, *Chem. Rev.*, 2014, **114**, 4041–4062.

10 V. Vasiliou, A. Pappa and D. R. Petersen, *Chem. Biol. Interact.*, 2000, **129**, 1–19.

11 K. Wang, B. Ma, S. Sun, X. Zhang, S. Lin and H. Tang, *ACS Sustain. Chem. \& Eng.*

12 F. Sun, L. Chen, X. Fan, Z. Meng and W. Liu, *J. Environ. Chem. Eng.*, 2025, 117590.

13 X. Wu, S. Wang, J. Fang, H. Chen, H. Liu and R. Li, *ACS Appl. Mater. \& Interfaces*, 2022, **14**, 38895–38904.

14 Y. Wang, M. Gong, H. Wang, G. Xiao, H. Su and J. Xing, *Photocatal. Res. Potential*,

2024, **1**, 10011.

15 G. Lin, Y. Zhang, Y. Hua, C. Zhang, C. Jia, D. Ju, C. Yu, P. Li and J. Liu, *Angew. Chemie Int. Ed.*, 2022, **61**, e202206283.

16 M. A. Emmanuel, S. G. Bender, C. Bilodeau, J. M. Carceller, J. S. DeHovitz, H. Fu, Y. Liu, B. T. Nicholls, Y. Ouyang, C. G. Page and others, *Chem. Rev.*, 2023, **123**, 5459–5520.

17 H. Zheng, Z. Huang, P. Wei, Y. Lin, Y. Cao, X. Zhang, B. Zhou and C. Peng, *ACS Sustain. Chem. Eng.*, DOI:10.1021/acssuschemeng.4c10134.